NASA TECHNICAL NOTE

NASA TN D-3421

EXPLORATORY STUDY OF PERFORMANCE OF THE LANGLEY PILOT MODEL EXPANSION TUBE WITH A HYDROGEN DRIVER

by Jim J. Jones and John A. Moore

Langley Research Center
Langley Station, Hampton, Va.

NATIONAL AERONAUTICS AND SPACE ADMINISTRATION • WASHINGTON, D. C. • MAY 1966

EXPLORATORY STUDY OF PERFORMANCE OF THE LANGLEY PILOT MODEL EXPANSION TUBE WITH A HYDROGEN DRIVER

By Jim J. Jones and John A. Moore

Langley Research Center
Langley Station, Hampton, Va.

NATIONAL AERONAUTICS AND SPACE ADMINISTRATION

For sale by the Clearinghouse for Federal Scientific and Technical Information
Springfield, Virginia 22151 – Price $2.00

EXPLORATORY STUDY OF PERFORMANCE OF THE LANGLEY PILOT MODEL EXPANSION TUBE WITH A HYDROGEN DRIVER

By Jim J. Jones and John A. Moore
Langley Research Center

SUMMARY

An exploratory investigation has been made of expansion-tube flows using an unheated hydrogen driver, and the performance is compared with previous theoretical calculations. Studies of the velocity of the several fronts, the static pressure, and the test-section pitot pressure were made and discrepancies from the elementary theory noted. These discrepancies were analyzed in terms of viscous and nonideal flow effects. The general conclusion of the investigation is that these effects do not seriously impair the usefulness of the facility as a tool in high-velocity flow research.

INTRODUCTION

Efforts to develop ground facilities which would simulate the flow conditions of reentering space vehicles, including real-gas effects, have been frustrated by two principal difficulties. These are the extremely high reservoir pressures and temperatures required and the problem of maintaining chemical and thermal equilibrium in the gas throughout the expansion in a nozzle. Both these difficulties are circumvented in ballistic range techniques, but new restrictions arise, principally that models must be small and simple, angle of attack near zero, and onboard instrumentation very limited.

The approaches to the problem which utilize a stationary model necessarily involve adding energy to the flow after it has been accelerated to supersonic speed. The extremely high reservoir enthalpy which results in large dissociation and ionization, and the very high reservoir pressures, are thus avoided.

One proposed technique to accomplish the above aims is the expansion tube. In references 1 and 2 the device is described and its theoretical performance capability is calculated. A distance-time diagram of the assumed flow model is shown in figure 1. The purpose of the program reported in this paper is to compare the experimental

performance of the expansion tube with theory, looking particularly for major discrepancies between the two which might be due to viscous effects, nonideal diaphragm rupture, finite chemical reaction rates, or three-dimensional-flow effects, none of which were considered in the theoretical analyses. An additional aim was to determine what improvements in instrumentation are required as compared with currently available instrumentation for shock-tube or shock-tunnel work.

Since the expansion tube is a direct extension of the shock tube, and could, in fact, be described as a modified buffered shock tube, a great deal of information as to actual performance is already available. However, in shock-tube flows it is usual to test in the gas immediately behind the shock wave, and the nature of the flow behind the interface has received relatively little attention, whereas in the expansion-tube flow this gas behind the interface is the test gas.

As a result of the knowledge gained in the study of shock tubes, several immediate questions arise as to the quality and limitations of the expansion tube flow. Among these are:

1. Attenuation.- It is well known that the growth of the boundary layer on the shock-tube wall generates a wave system which attenuates the shock wave and the flow. What is the magnitude of this attenuation in the expansion tube; how does it affect the steadiness of the state of the test gas during the testing period?

2. Secondary-diaphragm rupture.- The strength of the secondary diaphragm is assumed to be just sufficient to avoid premature rupture, and the elementary theory assumes that the diaphragm ruptures instantaneously upon shock impingement without subtracting momentum from the flow. In actual operation, however, some margin of safety is necessary in the diaphragm strength to avoid premature rupture, and the diaphragm mass is not zero, so some momentum must be subtracted from the flow unless the diaphragm is ruptured by external means. In reference 3 it is shown that the mechanism for extracting the necessary momentum from the flow is an upstream-facing shock wave. Determination of the strength of this shock wave and its effect on the subsequent flow thus becomes important.

3. Flow turbulence.- Since the test flow has passed over the ruptured diaphragm, and shock-tube studies indicate that such flow may be quite turbulent, the level and scale of this turbulence is subject to question.

4. Interface mixing.- If the test gas mixes extensively with the acceleration-chamber gas at their interface, a very deleterious effect on useful testing time could result. In conventional shock-tube flow, where the densities on the two sides of the interface are frequently of the same order, and where the strong primary diaphragm may have taken several hundred microseconds to open fully, many investigators have noted

severe interface mixing. Some study of this problem must be made in the expansion tube to determine the extent of its severity.

5. Interface position.- Several investigators (for example, refs. 4 to 6) have shown that in low-density shock-tube flows the boundary layer captures a large fraction of the flow processed by the shock wave, and as a consequence the interface approaches much closer to the shock wave than one-dimensional theory would allow. References 7 to 9 have treated the problem theoretically and show reasonable agreement with results of air and argon shock experiments. The phenomenon should be evident for the low-density helium flow of the expansion tube and is important because of its effect on test-gas velocity and testing time.

6. Boundary-layer thickness.- The wall boundary layer grows with time at the test-section location. Its thickness and rate of growth will determine effective test core size.

7. Thermal and chemical nonequilibrium.- To what extent has the flow departed from thermal equilibrium in its rapid passage through the expansion fan? Although the dissociation level of the test gas behind the primary shock wave is quite small in comparison with the equivalent reservoir condition, the thermodynamic state and particularly the static temperature will be appreciably affected if the vibration and dissociation are essentially "frozen" during the expansion.

8. Effective test time.- The testing time, defined as the period for which undisturbed steady flow exists at the test-section location, cannot be treated as a separate consideration, since it is the result of the limitations imposed by many other factors, including those enumerated here. Achievement of a testing period sufficient to establish steady flow over a model and to permit instrumentation to respond is, of course, vital to the successful operation of the expansion tube.

Although complete answers to the questions have not been obtained, the present investigation explores the relative importance of these factors and indicates areas which need closer examination.

SYMBOLS

Measurements for this investigation were taken in the U.S. Customary System of Units. Equivalent values are indicated herein in the International System (SI) in the interest of promoting use of this system in future NASA reports.

a	speed of sound
h	flow static enthalpy

l	separation between helium shock wave and interface
M	flow Mach number
M_{S_1}	primary-shock Mach number
p	static pressure
p_t	pitot pressure
t	time
U_{S_1}	velocity of primary (air) shock wave
U_{S_2}	velocity of secondary (helium) shock wave
u	flow velocity
u_i	secondary interface velocity
u_l	limiting velocity of an unsteady expansion wave
x	distance from primary diaphragm
Z	reciprocal molecular weight, $\frac{\text{Undissociated molecular weight}}{\text{Dissociated molecular weight}}$
z	initial length of test gas slug in intermediate chamber
γ	specific heat ratio

Subscripts:

0	standard conditions at 1 atmosphere (101.325 kN/m^2)
1	initial state in intermediate chamber
2	state immediately behind primary shock wave
3	state immediately behind primary interface
4	

4 initial state in driver

5 state of test-gas flow

10 initial state in acceleration chamber

20 state behind secondary shock wave

Regions defined by subscripts are indicated in figure 1.

APPARATUS

The facility used for the present tests was a shock tunnel with the following modifications: (a) Installation of a second diaphragm section, (b) removal of the nozzle minimum section, and (c) installation of a new test section just upstream of the nozzle. With this arrangement the nozzle functions as a dump chamber.

A sketch showing the pertinent dimensions is presented in figure 2. The test section is merely a "free-jet" type with suitable model-mounting ports and windows to allow observation of the flow as it issues from the tube. A photograph of the test section is shown in figure 3.

The secondary diaphragm, which separates the intermediate chamber from the accelerating chamber, was positioned at two different locations during the present program. Initially it was located 24.65 feet (7.51 m) downstream of the primary diaphragm. This location is denoted "A" in figure 2. However, during the test program it appeared desirable to change the relative lengths of the last two chambers and so the diaphragm was moved to a location 35.86 feet (10.92 m) from the primary diaphragm. This location is designated "B" in figure 2.

Mechanical vacuum pumps and diffusion pumps were connected to the nozzle dump tank through a manifold and these were used to evacuate the dump tank and acceleration chamber to approximately 10^{-4} torr (1 torr = 133.3 N/m^2). Helium was admitted to the acceleration chamber through a port located just downstream of the second diaphragm. At low values of p_{10} an attempt was made to minimize the effects of leakage and outgassing by bleeding in helium continuously and balancing the flow with a vacuum pump so as to achieve the desired pressure p_{10}. Both the helium valve and the vacuum valve were closed a few seconds prior to the run. At higher values of p_{10} (0.1 torr and above) the percentage of impurities was expected to be low, so the vacuum pump valves were closed after initial evacuation and the chamber was merely filled to the desired pressure.

The driver chamber and intermediate chamber were initially evacuated with mechanical vacuum pumps before filling with hydrogen and air, respectively.

INSTRUMENTATION

Wave Detection

Several devices were used to detect wave passage and to measure flow quantities. The shock-wave passage through the test-gas chamber is, of course, typical of shock-tube operation, and standard ionization gaps were used in conjunction with time-interval meters to monitor this shock velocity.

This technique is not, in general, satisfactory in the acceleration chamber because of difficulties in interpreting the resulting signal. Several devices have been tried to detect wave passage in the accelerating chamber. One is a flush-mounted pressure transducer, which is sensitive to the passage of the shock wave traveling in the helium but will not detect interface passage. It should, at least ideally, detect the passage of the tail of the expansion wave.

Photomultipliers have also been used, mounted outside the acceleration chamber. They were restricted to a small field of view normal to the tube axis and were thus able to detect the passage of any wave which emitted light within the limits of detectability of the photomultiplier. Figure 4 shows two sample records of the output of a photomultiplier and of a pressure transducer, both mounted at the same axial station. Figure 4(a) illustrates a case in which the photomultiplier detects both the helium shock and the helium-air interface. On many runs the shock wave was not detected by the photomultiplier; it is probable that the observed emission from the shocked gas is due to impurities, and thus the impurity level on a given run determines the photomultiplier's ability to "see" the shock passage. Figure 4(b) illustrates a low-density condition in which the shock and interface are so close together that they are not resolved by the photomultiplier. The sharp spike of light at the interface, shown in figure 4(b) as a break in the photomultiplier trace, was characteristic of most runs. The verification that this light is the interface was provided by the pitot pressure, which is discussed later.

The light output increases in the expansion fan, but attempts to identify the tail of the expansion wave with the photomultiplier signals have not yielded reliable results.

Pitot Pressure

Pitot-pressure measurements are sensitive to helium shock, interface, and expansion-wave arrival. In general, instrumenting the tube along its length with pitot probes would be unsatisfactory because of the resulting disturbance to the flow. However, a pitot probe mounted in the test section has served in the present tests to provide a positive identification of wave passage at the test-section location and thus confirm the results of other detectors described. A sample pitot-pressure record is shown in figure 5(a).

Several pitot-pressure probes and transducer models were tried in order to confirm the pressure histories obtained, provide protection for the transducer from particle damage, and obtain minimum response time. The most satisfactory design used is shown in figure 5(b). In this design, which is essentially a cylinder in cross flow, the transducer diaphragm is protected in that particles may strike it only after they have reflected off the cavity wall. The large orifice size, short length, and small cavity volume result in an aerodynamic response of about 10 μsec except for flow of very low density.

Microwave

A 2175-Mc microwave signal was propagated upstream into the acceleration chamber by means of an antenna mounted downstream of the test section. A moving reflector surface thus resulted in a varying antenna impedance. The necessary reflector movement between successive half-wavelength intervals was calculated to be 5.098 inches (12.949 cm) and this distance was confirmed by careful measurement of the movement of a wooden plug with an aluminum-foil face. Comparison of the microwave signal with data from other detectors (as in fig. 6) results in the conclusion that the microwave is reflected from the shock wave in the intermediate chamber and from the helium-air interface in the acceleration chamber for most run conditions. Since the strength of the microwave reflection is dependent on the electrical conductivity and therefore on the electron density, some ionization apparently is occurring at the helium-air interface. This is in accord with the photomultiplier signal, which shows a glowing region at the interface.

At low p_{10} (below 10^{-2} torr) the microwave signal did not track the helium-air interface but instead tracked a considerably lower velocity. For this reason it was deemed necessary to compare the microwave signal with other instrumentation on each run to be assured that the velocity record it obtained was meaningful.

TEST CONDITIONS

The driver gas used for the present program was room-temperature hydrogen. The primary diaphragm used in all runs was 1/16-inch-thick (0.159 cm) steel which resulted in a self-burst driver pressure p_4 of 1500 $\pm$ 200 psi (10.34 $\pm$ 1.38 MN/m^2).

The test gas was room air except for a few runs in which commercially bottled nitrogen was used. The secondary diaphragm was 0.00025-inch-thick (0.00635 mm) poly[ethylene terephthalate] plastic (PET). In order to study the effect of diaphragm strength a few runs were made with 0.0005-inch (0.01270 mm) and 0.002-inch (0.05080 mm) PET.

Three values of initial test-gas pressure p_1 were used: 22, 50, and 100 torr. The average measured shock Mach number and corresponding calculated equilibrium conditions behind the shock wave are summarized in the following table:

p_1, torr	M_{S_1}	p_2, atm	Z_2	h_2		u_2		u_l	
				Btu/lb	kJ/kg	ft/sec	m/sec	ft/sec	m/sec
22	8.3	2.49	1.025	1885	4381	8400	2560	28 800	8778
50	7.5	4.74	1.009	1608	3737	7500	2286	25 900	7894
100	6.7	6.98	1.00	1245	2893	6440	1963	22 060	6724

For each of the three initial shock conditions the acceleration-chamber pressure p_{10} was varied over a wide range. This procedure accomplished two purposes. First, at relatively high values of p_{10} reasonably accurate measurements of static pressure can be made; the boundary-layer growth is small, so the flow approaches the inviscid case and the interface is more easily located. Thus it is expected that although the velocity is low and static temperature is high as compared with the more fully expanded condition where atmospheric duplication is achieved, wave identification and flow-state determination will be firmer. Second, as the acceleration-chamber pressure is reduced on succeeding runs, a measure is provided as to how the pressure-velocity process actually proceeds through the expansion wave. Thus the "performance" of the expansion wave is monitored in some detail, rather than only the final expanded result being observed.

For each of the initial conditions runs were made in which p_{10} was 10^{-3} torr or lower. However, very limited information was obtained at these conditions because of the limitations of available instrumentation, so most of the data presented were obtained at $p_{10} = 5 \times 10^{-2}$ torr or above.

RESULTS AND DISCUSSION

Shock Wave in Air

The velocity of the shock wave as determined by the microwave signal is shown in figure 7 for three sample runs. Each datum point represents an average velocity over a distance of approximately 20 inches (0.5 m) as determined from the time interval for each four resonance points. The data show that the attenuation is not severe and is in good agreement with the attenuation study made in this facility some time ago (ref. 10). Only a small portion of the test gas processed by the shock wave actually traverses the test section during the testing time (length z in fig. 1). Therefore it may be assumed with good accuracy that the test gas is acted on by a shock wave of constant velocity equal to

its velocity just before impingement on the secondary diaphragm. Shock attenuation is not a matter of concern only with regard to variation of shock speed over the distance z, however; rather, it is a measure of the overall effect of the wave structure which is overtaking the test flow. If the attenuation is great, indicating that the overtaking waves are of considerable strength, then timewise variation of the flow properties during the test time must be anticipated.

Combustion at Interface

In hydrogen-driven shock tubes where the driven gas is air, the possibility exists that combustion will take place at the interface. For example, reference 11 reports interface combustion in a shock tunnel accompanied by large effects on reservoir conditions. Consequently it is of interest to determine whether combustion was present in the intermediate chamber in this investigation.

Figure 8 shows oscilloscope records of the output of a photomultiplier mounted just a short distance upstream of the secondary diaphragm, for air and nitrogen as test gas. For air at $p_1 = 22$ torr and $U_{S_1} = 9459$ ft/sec (2883 m/sec), the light intensity rises at the shock wave arrival (as verified by other instrumentation) and decreases rapidly as the interface passes. (See fig. 8(a).) Interface arrival is earlier than would be predicted by inviscid theory; the predicted time between shock and interface arrival was about $2\frac{1}{2}$ times that measured by the photomultiplier. Figure 8(b) shows a similar record for $p_1 = 50$ torr and $U_{S_1} = 8480$ ft/sec (2585 m/sec). The light intensity is only about 1/3 of that for the previous test condition (assuming linear response of the photomultiplier, which was not calibrated), and although the interface is discernible as a signal decrease, some light is present for the next 200 μsec. In figure 8(c), where $p_1 = 75$ torr and $U_{S_1} = 7870$ ft/sec (2399 m/sec), very little light is observed in the test gas, but the light increases at interface arrival, indicating that combustion was definitely present. Figure 8(d) is a record for nitrogen as the test gas, $p_1 = 50$ torr and $U_{S_1} = 8340$ ft/sec (2542 m/sec). Notice that the test-gas luminosity is much less than for a similar condition in air, and the light after interface arrival is completely absent.

As will be discussed later, no other important differences were noted when nitrogen was substituted for air; although combustion was present for some of the operating conditions, it did not produce any apparent effect on the test flow at the test section. Consequently the study of interface combustion was not pursued to determine the ranges of shock velocity and initial pressure for which it exists, or whether the mixing is sufficient to support continued combustion for long distances along the driven tube.

Helium Flow

The passage of the shock wave in helium in the acceleration chamber was detected by wall-mounted pressure transducers for high values of p_{10} and thus low shock Mach numbers. At low pressure, where the shock Mach number was somewhat higher, photomultiplier and ion gaps were satisfactory in verifying shock passage. The shock velocity was determined by plotting the pressure signals and/or photomultiplier signals on a large-scale distance-time diagram and measuring the slope of a line faired through the data points. Never more than five points and frequently as few as three points were available for determining the shock. Thus an accurate determination of the shock attenuation was not possible. For most runs a straight line fit the pressure data points fairly well, indicating that the attenuation was small. The accuracy of the data implies that the shock attenuation was less than 5 percent.

The pressure rise across the helium shock is presented in figure 9, where the measured pressure ratio p_{20}/p_{10} is shown as a function of shock velocity. The values presented for p_{20} are the wall pressure-transducer readings immediately following helium shock arrival. However, at low helium density the interface arrives at the measurement station a very short time after shock arrival (see fig. 4(b)), and for these cases presentation of the data required the assumption that $p_5 = p_{20}$. The perfect-gas theory shown should be very accurate for pure helium since the specific heats of helium are constant up to about 12 000° K, while the temperature range under consideration extends to only about 4000° K. The scatter of the experimental data and deviation from theory, particularly at the higher shock speeds which correspond to low values of initial pressure p_{10}, are thought to be due to: (1) the inaccuracy of the pressure transducer measurement p_{20}, which is estimated to be about ±0.1 psi (690 N/m^2); (2) the inaccuracy of the measurement of the initial pressure p_{10}, which contained several possible sources of error that could result in total errors of the order of 40 percent on some runs; and (3) contamination of the helium by leakage and outgassing, which would change the molecular weight and specific heats of the gas. In order to see the sensitivity of the pressure ratio to molecular weight, a theoretical curve is shown in figure 9 for a mixture of 7 percent air and 93 percent helium. Both helium and air were assumed to be perfect gases. This calculation shows that much of the deviation from pure helium theory can be attributed to leakage and outgassing.

Interface Velocity

As mentioned previously, the interface was tracked by the microwave signal and confirmed by the photomultiplier signal and pitot pressure. Samples of the velocity variation with distance are presented in figure 10. The data symbols represent the velocity determined by measuring the time interval for each two resonance peaks of the

microwave signal (Δx = 10.19 inches or 0.259 m). Figure 10 shows that the interface accelerates for approximately 3 feet (1 m) and then on some runs a relatively rapid attenuation is observed, after which only slight attenuation occurs.

Shock-Interface Separation

The separation between interface and shock wave in the acceleration chamber is expected to be much less than would be predicted by one-dimensional inviscid theory, because of the rapid boundary-layer growth in the low-density flow which results in what is commonly called the leaky piston effect. The theory of Mirels, reference 9, which includes boundary-layer development, is compared with the present data in figure 11, where the separation distance l is shown to decrease to very small values at low initial pressure p_{10}. Mirels' solution for a Prandtl number of 0.72 and $\gamma = 5/3$ was used. The data presented were obtained by plotting on an x-t diagram the experimental determination of shock and interface passage through the acceleration chamber, fairing curves through these points, and measuring the separation of the curves at a distance of 45 feet (13.72 m) from the secondary diaphragm. The data tend to indicate somewhat longer separation distances than theory, which is in contrast with most other data available: reference 9 indicates that the theory overpredicts the separation distance since mixing is not accounted for. The difference may be due to the large difference in diaphragm strength. In the present case the flow into the acceleration chamber is initiated by the rupture of a very light, weak diaphragm, whereas all other available data were obtained in shock tubes, where the diaphragm is normally much heavier and the opening times are therefore longer. Thus the mixing process which is promoted by the finite opening time may account for the earlier arrival of the interface in the shock-tube data.

The pitot-pressure measurements show quite clearly the duration of helium flow except where the duration was too short to permit the pitot probe to respond. The pitot pressure is much less in the helium than in the air following because of the difference in density. Figure 12 compares the calculated and measured values of $p_{t,20}$ for a wide range of initial pressure p_{10}. These data are subject to the same sources of error discussed in connection with the static-pressure measurements. The effect of 7 percent air contamination is again shown and could account for the fact that a number of the data points are higher than theory. No data are available for the highest velocity runs because at the low values of initial pressure p_{10} necessary to obtain high velocity, the duration of helium flow over the model was too brief to permit the pitot probe to respond. For the data shown in figure 12 the free-stream Reynolds number based on probe diameter ranged from 200 to 1000. Therefore no significant low-density effects on the pitot-pressure measurements should be present. For example, reference 12 indicates the low-density effect should be less than 3 percent.

Static-Pressure Measurements

Figure 13 presents the wall static pressure measured by the transducer just upstream of the test section as a function of the interface velocity u_i. As was shown in figure 4, the static pressure remained relatively constant until the arrival of the expansion fan. Therefore the value plotted is valid for the entire test period. The static pressures are lower than would be predicted by the ideal-performance theory, particularly for the conditions p_1 = 22 torr and 50 torr. Several possible causes for this difference have been examined and are shown in figure 13.

Perhaps the first consideration is whether equilibrium has been attained by the flow. Since the portion of the air flow that becomes the test flow was cooled extremely rapidly by the expansion fan, it appears likely that adjustment of the vibration and dissociation modes has not been permitted. This effect has been examined by calculating the limiting case of "freezing" the vibration and dissociation at the conditions behind the incident shock. This calculation is indicated by the curve in figure 13 marked "Frozen expansion."

The flow energy lost in the rupture of the diaphragm with finite strength and mass must result in an upstream-facing shock wave which would increase the entropy of the test gas. This shock wave was observed by Knöös and discussed in reference 3, where the shock was noted to be approximately a standing wave. In the present tests a pressure transducer was mounted in the wall of the tube 5/8-inch (1.6-cm) upstream of the secondary diaphragm to determine whether a reflected shock wave moved back up the intermediate chamber as a result of the diaphragm rupture process. The transducer detected no shock wave except when diaphragms four times the normal strength were used. Thus it was determined that for normal-strength diaphragms, 0.00025-inch (0.00635-mm) thick, the shock wave was not stronger than a standing wave. The effect of such a standing wave on the static pressure is indicated in figure 13 for both equilibrium and frozen expansion. The presence of the shock wave has only small effect if equilibrium expansion is assumed, but, as anticipated from the consideration of the increased dissociation, the "frozen" assumption results in large decreases in pressure for a given velocity. The static-pressure data are compatible with either the "shock" or "no shock" assumption if some intermediate nonequilibrium relaxation rate is assumed. However, each streamline of the test gas is cooled at a different rate by the expansion, the rate being slowest for the gas which arrives latest. Therefore a rising static pressure might be expected if significant relaxation were taking place in the expansion. The static-pressure measurements did not display this pressure rise.

One further attempt to correlate the data is illustrated in figure 13. As was shown in figure 10, the interface typically slows down 500 to 1000 ft/sec (150 to 300 m/sec) in traversing the length of the acceleration chamber. If this attenuation is the result of

downstream-facing expansion waves (commonly referred to as P-family waves) generated by the growing boundary layer upstream, then the usually constant quantity $u + \Delta u$ is decreased in the test gas. (The quantity Δu, which becomes $\frac{2}{\gamma - 1} a$ in a perfect gas, is discussed in reference 13 and values are presented for Δu as a function of enthalpy.) As is pointed out in reference 13, the limiting velocity $u_l = u + \Delta u$ remains unchanged through a Q-family expansion and therefore has the same value in the test gas as it had immediately behind the shock wave in the intermediate chamber. The calculated result of assuming that the gas has been intercepted by sufficient P-family expansions to cause a 1000 ft/sec (305 m/sec) decrease in flow velocity is shown in figure 13. It was assumed that the gas was in equilibrium throughout and no upstream shock existed. The calculation was made by assuming that any given stream tube was first expanded to a given velocity by the Q-family expansion ($u + \Delta u$ = Constant) and subsequently decreased in velocity by 1000 ft/sec (305 m/sec) due to P-family expansions ($u - \Delta u$ = Constant). Since the final amount of expansion corresponding to a velocity change of 1000 ft/sec (305 m/sec) is a deceleration (P-family) expansion rather than an acceleration (Q-family) expansion, the test-gas velocity is reduced 2000 ft/sec (610 m/sec) for any given test-gas pressure; that is, the 1000 ft/sec (305 m/sec) reduction of the P wave plus the 1000 ft/sec (305 m/sec) which would have accompanied a Q wave of comparable pressure drop).

A certain amount of scatter in the static-pressure measurements must be attributed to variations in the shock speed U_{S_1} from run to run. In eliminating this source of scatter the static-pressure data of figure 13 have been standardized to an average shock Mach number, so that all the data at a given initial pressure p_1 can be compared with theoretical calculations for a given shock Mach number M_{S_1} corresponding to the experimental average. The formula used was

$$p_{corr} = p_{exp}\phi$$

where

p_{corr} corrected value of experimental pressure

p_{exp} measured value of experimental pressure

ϕ ratio of the calculated pressure using the standard shock Mach number to the calculated pressure using the experimental shock Mach number, each evaluated at the experimental interface velocity

The simple equilibrium theory assuming no reflected shock was used for the calculation of the correction to the pressure. In most cases the correction was small, and for two-thirds of the data it was less than 10 percent.

Pitot-Pressure Measurements

The state of the expanded gas can be examined further with the aid of the pitot-pressure measurements $p_{t,5}$ as presented in figure 14. The calculated values of pitot pressure for the several different assumptions discussed previously are also shown in figure 14. A standardizing process similar to that previously described was applied to the pitot pressures. In all cases the pitot pressures appear to be low, and in comparison with the calculated curves, are lower than the corresponding static-pressure measurements. This is seen more clearly in figure 15, where the pitot-pressure measurements are plotted against the static-pressure measurements and compared with the theoretical calculations. Presented in this form, the data show the best agreement with the calculation which includes the effect of the attenuation P-family expansions. The agreement is still not good, but the figure seems to indicate that "freezing" of the relaxation in the expansion is not a suitable explanation for the trend of the data. An analytical study of the relaxation of air in the unsteady expansion fan is currently being conducted to determine what deviation from thermal equilibrium might be expected in the expansion-tube test flow.

Figure 16 shows the character of the pitot pressure for a wide range of initial pressure p_{10}. The traces are the transducer amplifier output after being filtered to attenuate oscillations above 10 000 cps (10 000 hertz). An unexpected dip or decrease is evident in the curves. The dip is easily observed at high values of p_{10} and seriously decreases the test time (period of constant conditions). At low values of p_{10} the dip does not arrive until after the tail of the expansion fan and so it is not so easily observed. In figure 16(c), for example, the pitot pressure remains constant for approximately 200 microseconds after the theoretical time for expansion-fan arrival, which is indicated by the arrow. This constant pressure might be construed as the result of the opposing effects of the dip and the expansion fan. In figure 16(d) a dip appears in the fan, beginning at about 2.2 milliseconds. The cause of the dip has not been determined definitely although a number of tests have been made to study its origin. It is apparently aerodynamic, since studies of the acceleration and heat sensitivity of the transducer have produced negative results. In support of this conclusion is the fact that streak photographs of the shock stand-off distance have shown that the bow-shock waves moved outward upon arrival of the dip.

The arrival of a downstream-facing wave, such as might be generated from the interaction of the driver-air interface with the leading edge of the expansion (see fig. 1), appears as a possible cause of the dip. If the driver-air interface is taken to be that

indicated by the photomultiplier signals in the intermediate chamber (fig. 8), the predicted arrival time of this reflection wave is in approximate agreement with the dip in the pitot pressure. Note that the time scale of figure 16 has its origin at the instant of secondary-diaphragm rupture and the dip arrival is approximately at the same time regardless of the initial pressure p_{10}, as would be expected from a downstream-facing wave. The use of nitrogen as the test gas caused no apparent change in the nature of the pressure dip, so it does not appear to be due to combustion at the interface.

If the cause of the dip is indeed a downstream wave, it should appear on the static-pressure records as well as on the pitot-pressure records. An approximate analysis of the expected change in static pressure as a function of the change in pitot pressure generated by a P-family wave results in the relation

$$\frac{dp_t}{p_t} \approx \frac{1}{\gamma}\left(1 + \frac{2}{M_5}\right)\frac{dp_5}{p_5}$$

Thus the static-pressure change should be of the same order as the pitot-pressure change. Such severe dips in static pressure have not been observed, however. The sample static-pressure record of figure 4 is typical of the maximum dips observed, which are on the order of 25 percent. The corresponding pitot pressure for the same initial conditions is figure 16(b), where the dip is about 50 percent. However, a static-pressure transducer mounted just upstream of the test section displays an increase in noise at the same time the dip in pitot pressure begins. The frequency of this noise is apparently the natural frequency of the transducer. The noise amplitude on the pitot-pressure transducer also increases at the same time. The phenomenon is discussed further in the section on flow turbulence.

The possibility exists that the dip in pitot pressure is due to the presence of helium in the flow. The boundary layer on the tube walls has accepted most of the helium which has passed through the shock wave. If some phenomenon, such as large-scale turbulence, were to cause the helium to return to the center stream, the result would probably be a decreased pitot pressure, increased shock stand-off distance, and decreased gas-cap luminosity. These effects are all observed concurrently, but as yet helium has not been identified in the gas cap at the time of the dip.

All pitot-pressure measurements presented in figure 14 were determined from the constant-pressure plateau preceding the dip. However, since the origin of the dip has not been definitely determined, it cannot be shown conclusively that they are free of such extraneous effects. The unexpectedly low values of pitot pressure prior to the dip (and in fact the dip itself) may possibly be caused by contamination of the test gas by helium. No definitive tests have as yet been made to determine the helium content of the test gas.

However, the very rapid rise of the pitot pressure at interface arrival (fig. 5(a), for example) would seem to argue against a thick, diffuse interface.

Flow Turbulence

As stated in the introduction, the turbulence of the test flow is subject to question because of the well-known high-turbulence level of shock-tube driver flow. No direct study of flow-turbulence level has been made in this investigation, but an indication of flow turbulence may be provided by the transducer "noise" of the pitot-pressure measurements. Figure 17(a) presents an unfiltered pitot-pressure record obtained in the expansion tube which illustrates the high-frequency noise observed. There is a rather sudden increase in the amplitude approximately 350 microseconds after interface arrival. Figure 17(b) shows pitot-pressure traces obtained with the same transducer in a conventional shock-tube flow. The initial pressure of the air in the driven tube was selected to approximate the same pitot pressure as the test flow in the expansion-tube run of figure 17(a). The calculated free-stream Reynolds numbers were 3×10^5 for the expansion-tube test gas and 2.6×10^5 for the shock-tube run. On the shock-tube record, figure 17(b), the interface arrives approximately 200 microseconds after the shock wave, which accounts for the sudden change in pitot pressure. If the gage oscillations are assumed to be due to a coupling with a portion of the turbulence spectrum of the flow, then figure 17 shows that initially the expansion-tube flow has no higher turbulence level than a corresponding flow behind a shock wave and that the turbulence level increases at some later time, after the testing period.

The study remains to be made of the effect of varying flow conditions on the time of arrival of the increased-amplitude oscillations. However, the static-pressure transducers also have their natural frequency excited rather abruptly, and as shown in figure 18, this excitation agrees in time with the pitot-pressure excitation. An ion gap mounted near this static-pressure transducer showed an increase in noise at the same time as the pressure transducers. Also illustrated in figure 18 is the fact that the dip in pitot pressure appears to be associated with this excitation. Thus one might speculate that the dip is due to boundary-layer transition. It is not clear at present why boundary-layer transition should cause a large decrease in center-line pitot pressure while creating only a small decrease in wall static pressure, and this matter is the subject of further investigation.

Streak-Camera Measurements

Measurements of the variation in shock stand-off distance with time were made by using a streak camera with a 0.020-inch (0.05-cm) slit in front of it. An image of the glowing shock layer on the nose of the model (the pitot probe of fig. 5(b)) was focused on

the slit which was alined parallel to the flow direction. Thus the breadth of the light column passing through the slit and falling on the film drum was proportional to the shock stand-off distance. The film drum, whose axis was parallel to the slit, rotated at a peripheral speed of 2 inches per millisecond (5 cm/msec). The results of this study are illustrated by the sample runs shown in figure 19, where the streak-camera records are reproduced to the same time scale as the corresponding pitot-pressure records.

Figure 19(a) illustrates a condition in which the pitot-pressure dip occurs shortly after interface arrival. The following points are worthy of note.

1. No glow is detectable during the time of helium flow over the model. A photomultiplier focused on the shock layer confirmed that intensity of its glow in helium was less than 1 percent as great as the intensity of the shock-layer glow in air.

2. The shock stand-off distance increased as the pitot-pressure dip began.

3. The intensity was greatly decreased during the minimum of the dip. This was also confirmed by the photomultiplier.

Figure 19(b) was obtained on a run in which the secondary diaphragm was of wax paper. The wax paper tended to leak air from the intermediate chamber into the acceleration chamber. The resulting concentration gradient in the acceleration gas caused a gradually rising pitot pressure, a gradually increasing shock-layer intensity, and a gradually decreasing shock stand-off distance. This run, which in other respects was of little value, served to illustrate the predictable fact that the stand-off distance is considerably less in air than in helium and the shock must retreat to its new position upon interface arrival.

Figure 19(c) illustrates a run in which the pitot-pressure dip occurred somewhat later, after a period of relatively constant pitot pressure and stand-off distance. In the later portion of the run the stand-off distance varies erratically, in a pulsating manner. This effect was observed to some degree in all runs. These pulsations on the streak-camera record correlate quite well with the highest amplitude pulses in the pitot pressure, a fact which helps substantiate the assumption made in the previous section that the pitot pulsations are aerodynamic in nature rather than mechanical accelerations induced in the model support. It is not clear, however, whether these pulsations are caused by stream turbulence or by the arrival of secondary-diaphragm particles.

The initial portion of the streak photograph of figure 19(c) has been enlarged in figure 19(d). (In all the streak pictures of fig. 19 the leading edge of the model has been accentuated by marking a black line on the photograph.) This record shows that upon interface arrival the glow region proceeds outward from the body. The cause of this phenomenon has not as yet been explained or examined in detail.

Effective Test Time

Test times in the range of 100 to 400 microseconds were measured in the present investigation. In an expansion tube the test flow time is the period between the arrival of the helium-air interface and the tail of the expansion fan at the test section. As has been shown previously, the interface arrival is predicted moderately well by the "leaky piston" theory of reference 9. The end of the test period (the arrival of the expansion fan) is indicated by the static-pressure records. In practice, however, this measurement is difficult to determine within the accuracy that will provide meaningful data.

The sample static-pressure record of figure 4 illustrates the difficulty in determining the instant that the pressure starts to rise, corresponding to the arrival of the expansion fan. The best estimates of expansion-fan arrival at the several static-pressure locations were plotted on a large-scale distance-time diagram, and the slope of a line faired through these points was used to determine the velocity $u_5 - a_5$. Subtracting this from the flow velocity u_5 as determined by the microwave signal yields an experimental value for the test-gas speed of sound a_5. Note the implicit assumption that the test-gas velocity u_5 is the same at the front of the test-gas slug (interface) as it is at the rear (expansion tail).

The experimental sound speeds determined by the method just described are presented in figure 20. The data have a precision of only about ±800 ft/sec (244 m/sec) for the reasons described and display a large amount of scatter. The trend of the data is not well predicted by the theoretical calculations, however. The data for the most fully expanded cases (highest velocity) show a higher sound speed and therefore a longer test time than predicted by any of the theoretical calculations. The extreme underexpanded cases (lowest velocity) exhibit an unexpectedly low sound speed, particularly at $p_1 = 100$ torr, figure 20(c). No satisfactory explanation for these deviations from the calculated curves is currently available. Also it should be noted that there is poor agreement between the static temperature inferred from the sound-speed measurements and that which can be inferred from the measurements of static pressure, pitot pressure, and interface velocity.

CONCLUSIONS

An experimental investigation of the performance of a hydrogen-driven expansion tube has been made in order to compare the performance with predictions of previous analytical studies and to determine which aspects of the flow require more detailed study. The experimental program was conducted at three values of initial shock Mach number, and for each of these the initial acceleration-chamber pressure was varied over a wide range in order to vary the amount of expansion of the shocked flow. The quantities

measured were the velocities of the primary shock wave, the secondary (helium) shock wave, the secondary interface, and the tail of the expansion fan, as well as the wall static pressure and the test-section pitot pressure. The following conclusions have been reached:

1. The attenuation of the primary shock wave and the secondary interface are well within tolerable limits. However, the downstream-facing waves which produce the decay in interface velocity have a noticeable effect on the static and pitot pressures at the test section, and prediction of these quantities is improved if their effect is accounted for.

2. Because of the low density of the (helium) acceleration gas, the so-called "leaky piston effect" is large and draws the helium shock and interface quite close together. The laminar theory of Mirels slightly underpredicts the spacing between these fronts in the range of the present conditions. The importance of the leaky piston effect in expansion-tube flow is that the initial acceleration-gas flow over the model will be much briefer than would be predicted by inviscid theory.

3. The measured values of static pressure and pitot pressure in the helium flow displayed considerable scatter and tended to be higher than theoretical values. This was believed to be due chiefly to a lack of purity of the helium in the acceleration chamber. It was shown that a contamination of 7 percent air in the acceleration chamber would explain the discrepancy in many runs.

4. The measured static pressure in the test region was shown to be somewhat lower than the value calculated by elementary theory for the same flow velocity. The corresponding measured pitot pressures showed an even greater deviation from theory, and in many cases were only about one-half the calculated value. Several possible causes were examined, among them the attenuation of the expanded flow. While inclusion of this effect alone did not provide completely satisfactory correlation, it appeared to be the dominant source of discrepancy.

5. An unexpected dip is encountered in pitot-pressure records. Its time of arrival relative to the test flow is dependent on initial conditions. Further, the static-pressure records as well as the pitot-pressure records show a marked increase in the amplitude of the transducer oscillations at the instant of dip arrival. It is suggested that this dip might be related to boundary-layer transition and more study is warranted in this area.

6. If flow turbulence is assumed to be the cause of the undamped transducer oscillations and if the amplitude of these oscillations is assumed to be proportional to turbulence level, the turbulent level of the test gas flow, prior to dip arrival, is not greater than that of the shock accelerated flow in a shock tube for corresponding Reynolds number and pitot pressure.

7. Attempts to determine the test-gas sound speed by measuring the velocity of the tail of the expansion fan have resulted in rather large scatter, as might be expected when examining the small difference between two large experimental velocities. However, the mean of the data points indicates that the speed of sound is of the order of the calculated values, and therefore the available testing time is approximately as calculated. This conclusion applies only when the test time is not truncated by the pitot-pressure dip. Test times range from 100 to 400 microseconds in the present experiments.

A general conclusion derived from the present investigation is that the expansion tube produces a useful test flow whose velocity, duration, and thermodynamic state are of the order calculated by elementary theory. While differences from this elementary theory have been noted, and dictate further study, it appears that the expansion tube is a suitable facility for productive high-velocity flow research.

Langley Research Center,
National Aeronautics and Space Administration,
Langley Station, Hampton, Va., January 17, 1966.

REFERENCES

1. Trimpi, Robert L.: A Preliminary Theoretical Study of the Expansion Tube, a New Device for Producing High-Enthalpy Short-Duration Hypersonic Gas Flows. NASA TR R-133, 1962.

2. Trimpi, Robert L.: A Preliminary Study of a New Device for Producing High-Enthalpy, Short-Duration Gas Flows. Advances in Hypervelocity Techniques, Arthur M. Krill, ed., Plenum Press, 1962, pp. 425-451.

3. Knöös, Stellan: A Theoretical and Experimental Study of the Opening of the Low-Pressure Diaphragm in a Double-Diaphragm Shock Tube. Thesis, Roy. Inst. Technol. (Stockholm), 1963.

4. Duff, Russell E.: Shock-Tube Performance at Low Initial Pressure. Phys. Fluids, vol. 2, no. 2, Mar.-Apr. 1959, pp. 207-216.

5. Brocher, E. F.: Hot Flow Length and Testing Time in Real Shock Tube Flow. Phys. Fluids, vol. 7, no. 3, Mar. 1964, pp. 347-351.

6. Graber, Bruce C.; and Nerem, Robert M.: Test Duration Measurements in an Arc-Driven Hypervelocity Shock Tube. Rept. 1573-2 (Contract AF 33(657)-10523), Ohio State Univ. Res. Found., Oct. 15, 1963.

7. Roshko, Anatol: On Flow Duration in Low-Pressure Shock Tubes. Phys. Fluids, vol. 3, no. 6, Nov.-Dec. 1960, pp. 835-842.

8. Hooker, William J.: Testing Time and Contact-Zone Phenomena in Shock-Tube Flows. Phys. Fluids, vol. 4, no. 12, Dec. 1961, pp. 1451-1463.

9. Mirels, Harold: Test Time in Low-Pressure Shock Tubes. Phys. Fluids, vol. 6, no. 9, Sept. 1963, pp. 1201-1214.

10. Jones, Jim J.: Experimental Investigation of Attenuation of Strong Shock Waves in a Shock Tube With Hydrogen and Helium as Driver Gases. NACA TN 4072, 1957.

11. Copper, John A.: Effects of Interface Combustion and Mixing on Shock-Tunnel Conditions. AIAA J. (Tech. Notes), vol. 2, no. 9, Sept. 1964, pp. 1669-1671.

12. Bailey, A. B.; and Boylan, D. E.: Some Experiments on Impact-Pressure Probes in a Low-Density, Hypervelocity Flow. AEDC-TN-61-161 (Contract No. AF 40(600)-800 S/A 24(61-73), Arnold Eng. Develop. Center, Dec. 1961.

13. Grose, William L.; and Trimpi, Robert L.: Charts for the Analysis of Isentropic One-Dimensional Unsteady Expansions in Equilibrium Real Air With Particular Reference to Shock-Initiated Flows. NASA TR R-167, 1963.

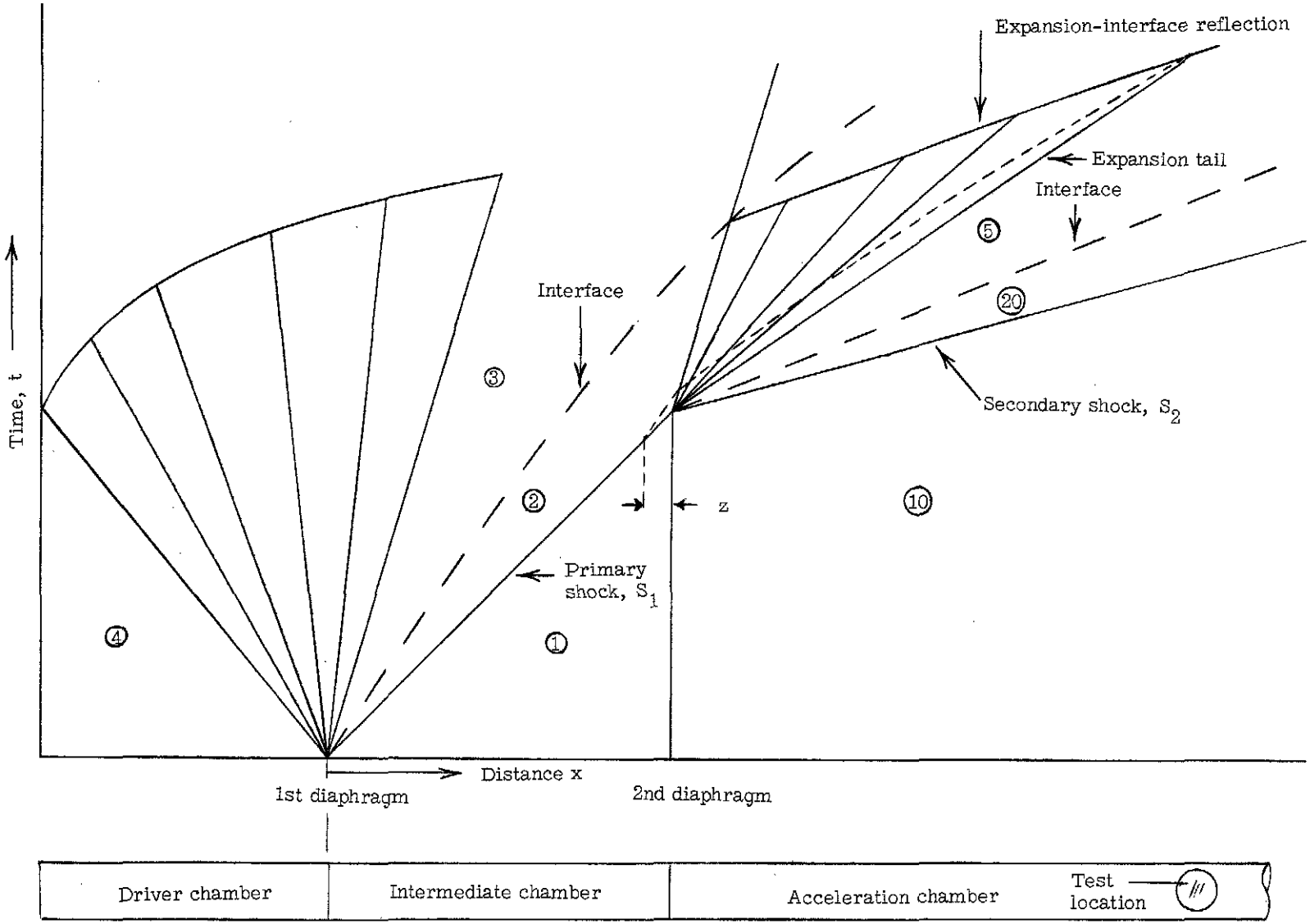

Figure 1.- Distance-time diagram of expansion-tube flow cycle showing pertinent flow regions.

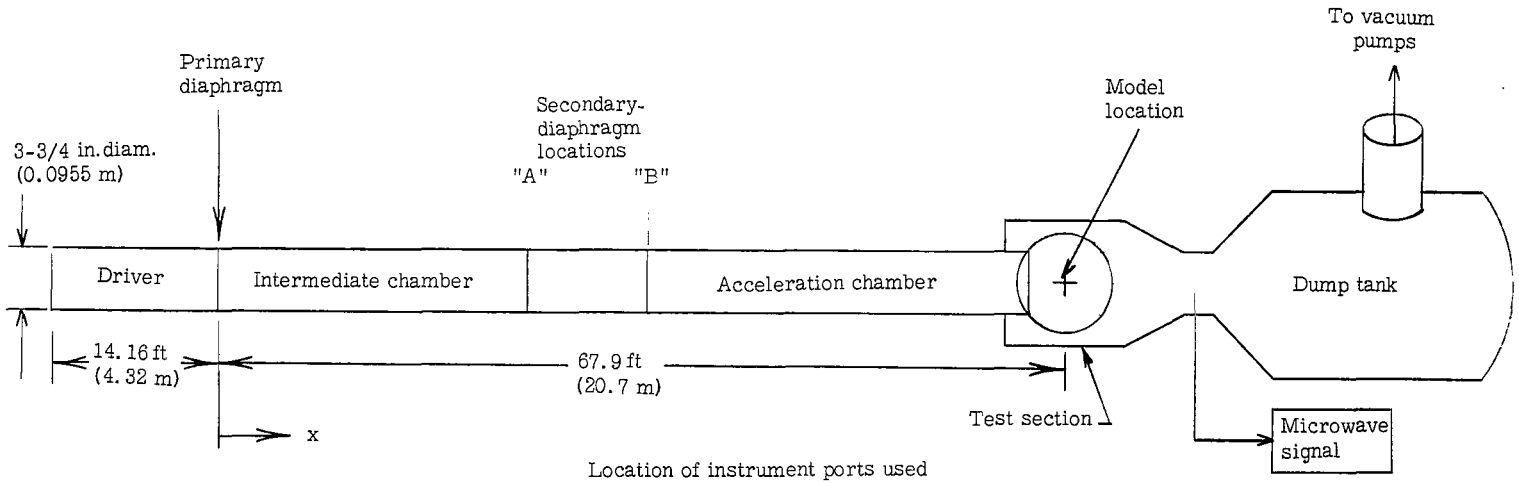

Location of instrument ports used

x	
ft	meters
4.62	1.41
6.62	2.02
8.62	2.63
10.62	3.23
12.16	3.71
17.86	5.44
23.38	7.12
29.10	8.86
34.61	10.55
37.46	11.41
46.25	14.10
50.84	15.50
62.50	19.05
67.50	20.58

Figure 2.- Sketch of Langley pilot model expansion tube.

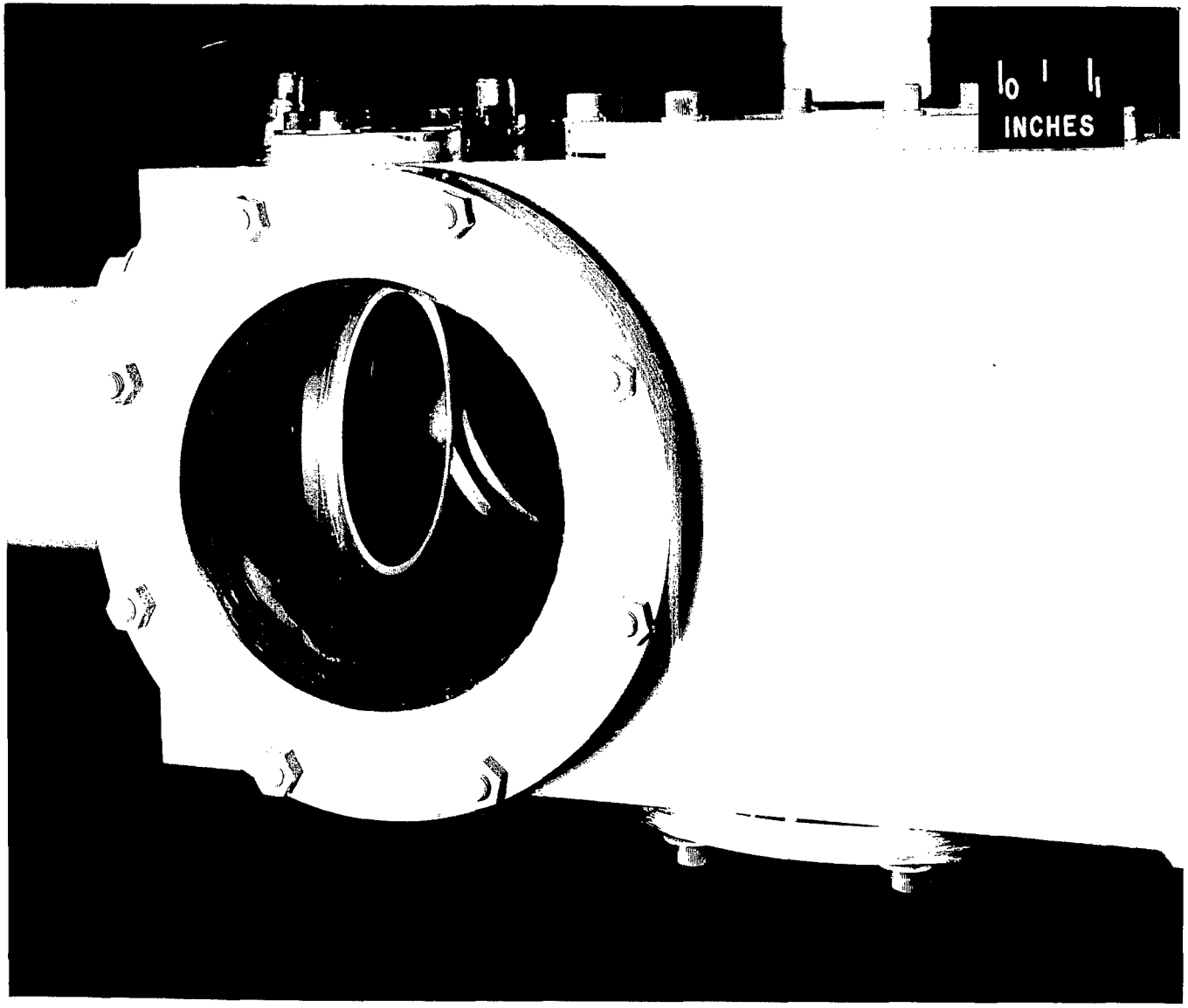

Figure 3.- Photograph of test section.

L-65-2186

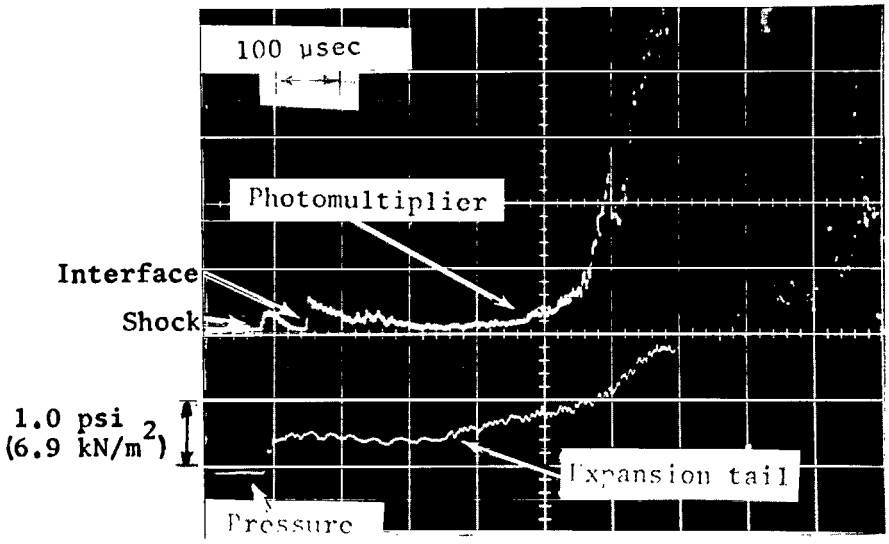

(a) p_{10} = 1.0 torr = 133.322 N/m^2.

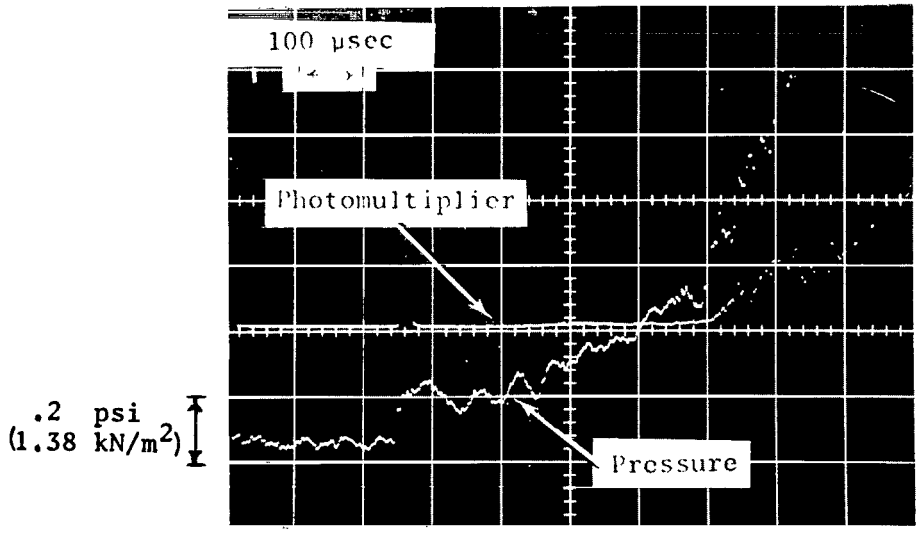

(b) p_{10} = 0.105 torr = 13.999 N/m^2.

Figure 4.- Examples of wall static pressure and photomultiplier traces in the acceleration chamber.

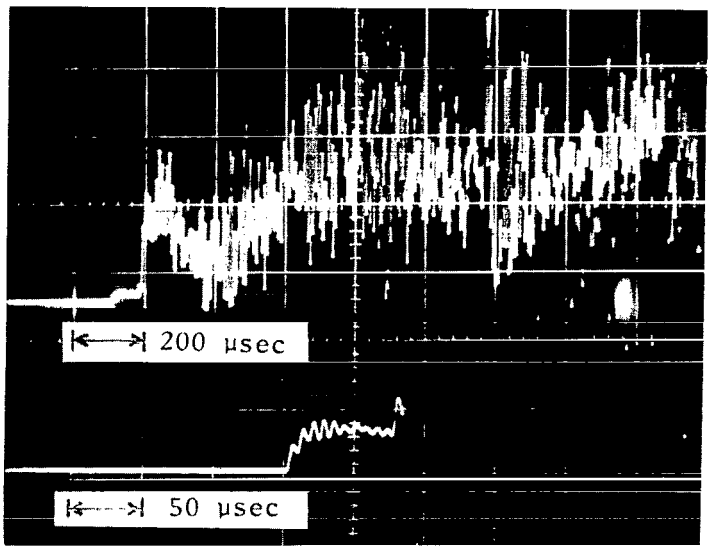

(a) Pitot-pressure record displayed at two different gains and sweep speeds.

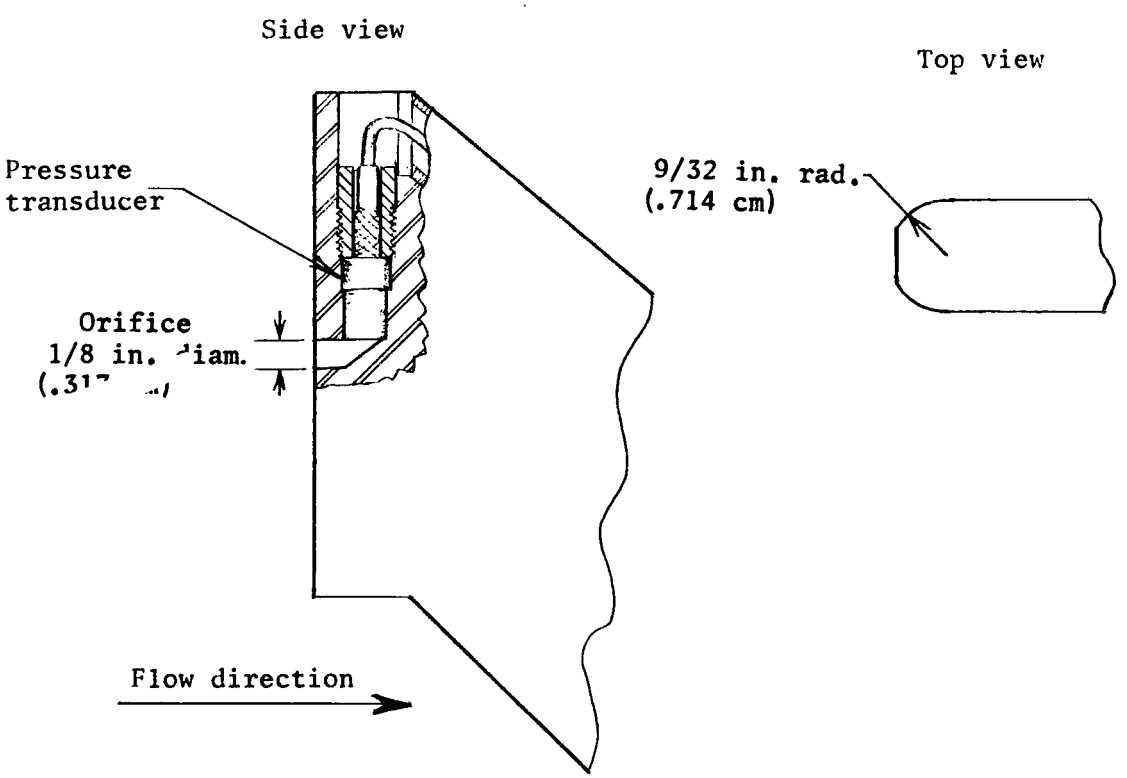

(b) Sketch of pitot probe which protects transducer from particle impact.

Figure 5.- Sample pitot-pressure traces and sketch of pitot probe.

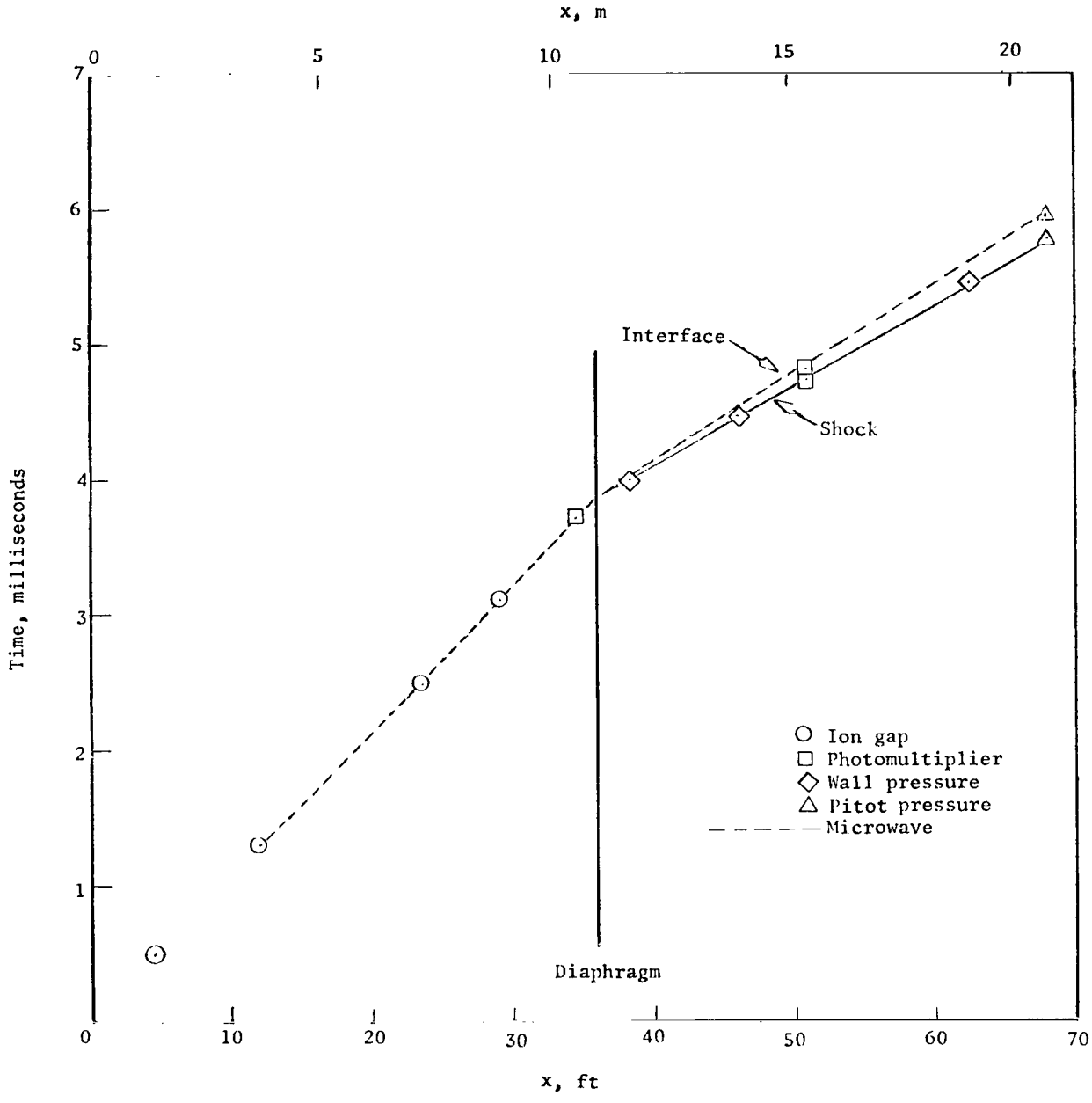

Figure 6.- Example of distance-time diagram showing correspondence of microwave signal with other wave-detection instrumentation.

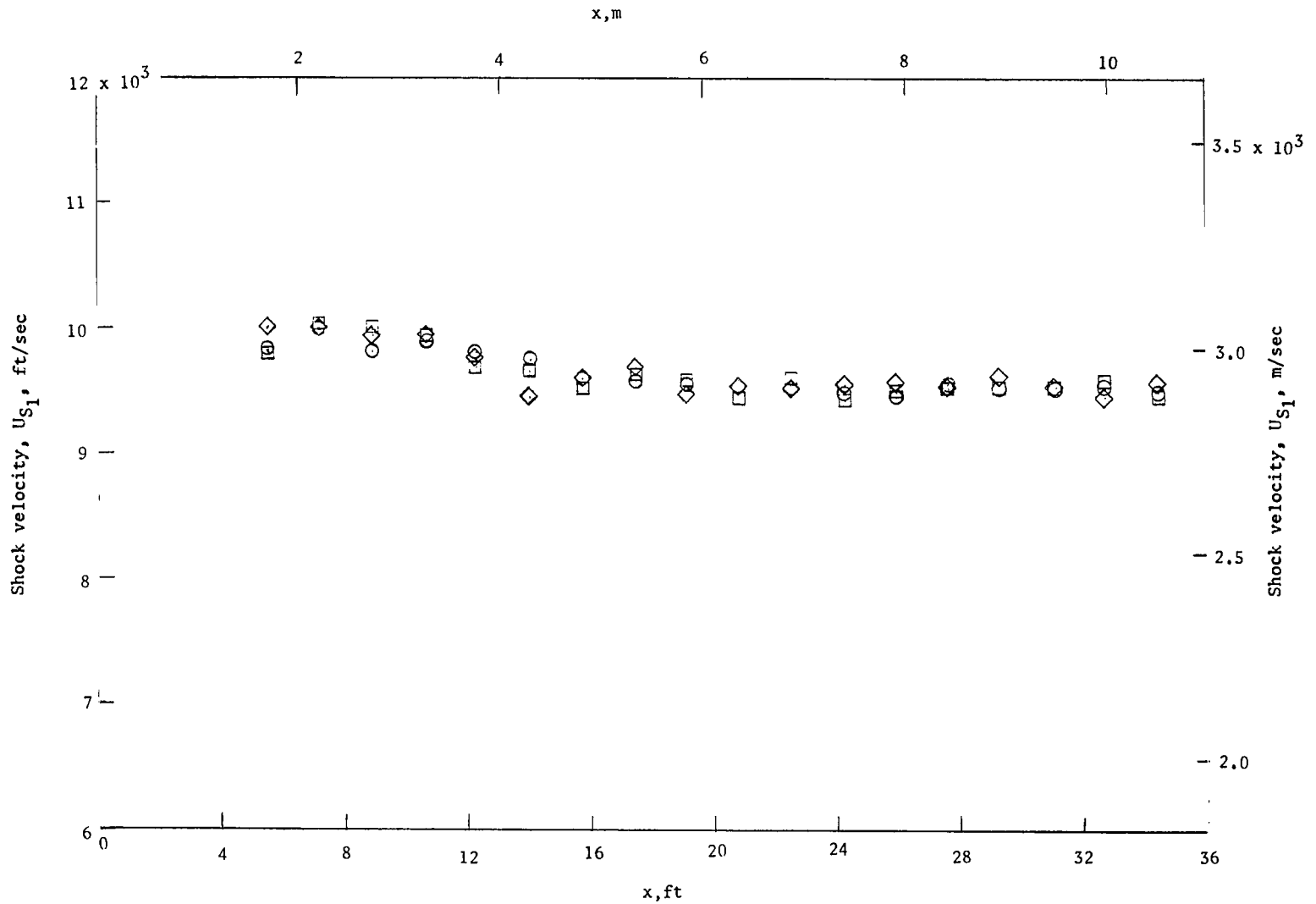

Figure 7.- Primary shock velocity of three typical runs, as shown by different symbols. p_1 = 22 torr = 2933 N/m^2.

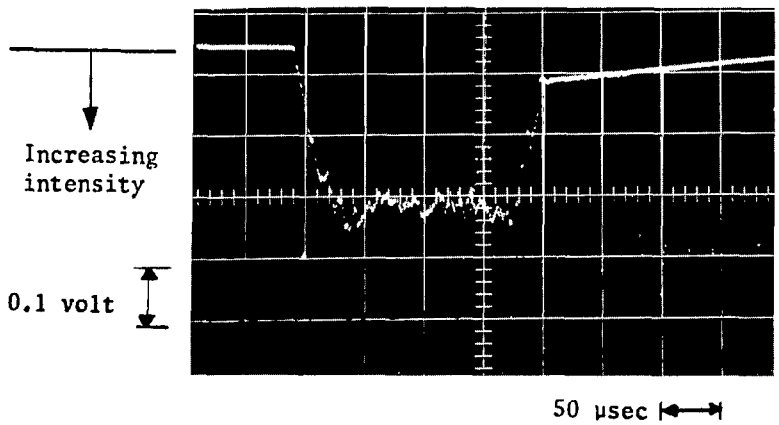

(a) Air; p_1 = 22 torr = 2933 N/m^2.

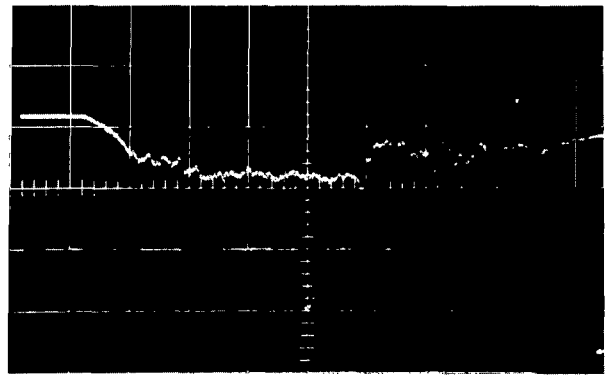

(b) Air; p_1 = 50 torr = 6666 N/m^2.

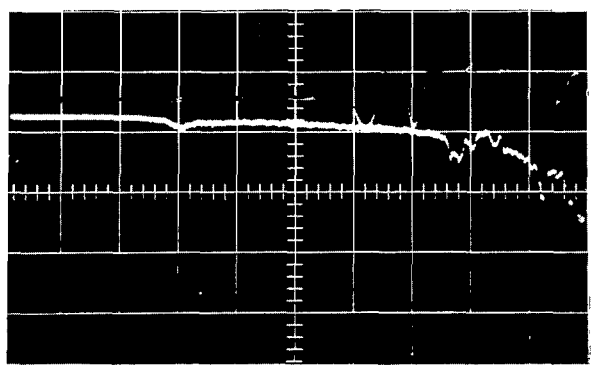

(c) Air; p_1 = 75 torr = 9999 N/m^2.

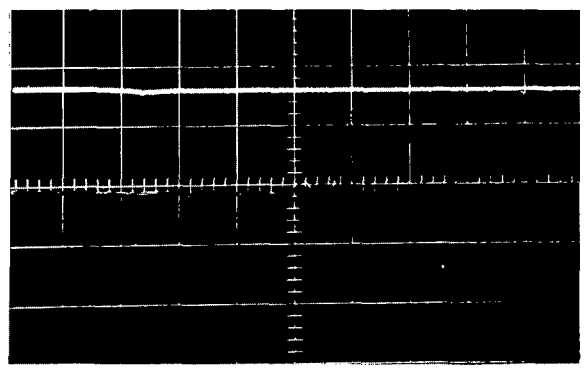

(d) Nitrogen; p_1 = 50 torr = 6666 N/m^2.

Figure 8.- Photomultiplier in wall of intermediate chamber. Gain and sweep are same for all oscillograms (oscillograms have been retouched to remove trace not discussed).

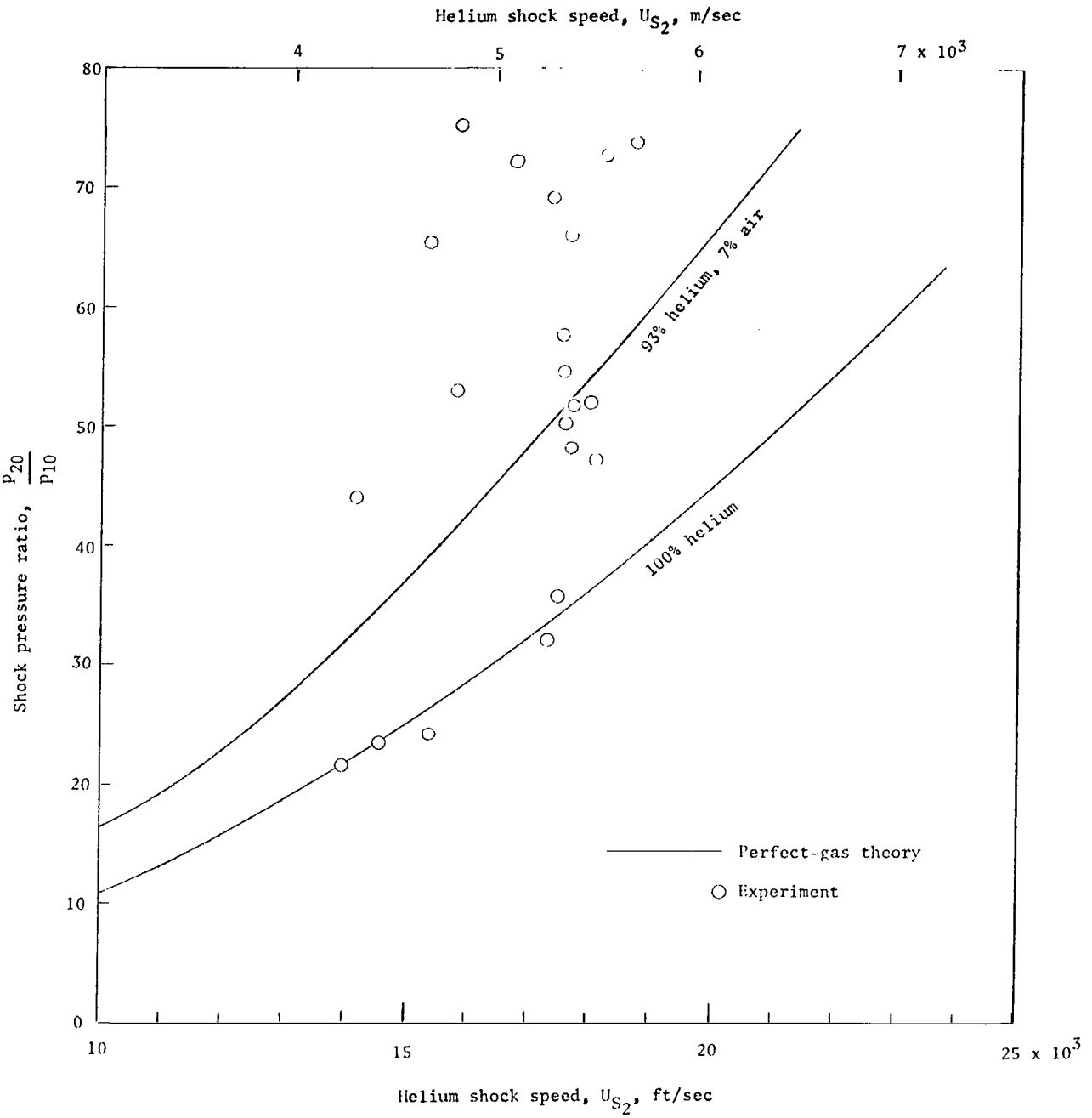

Figure 9.- Pressure ratio across helium shock.

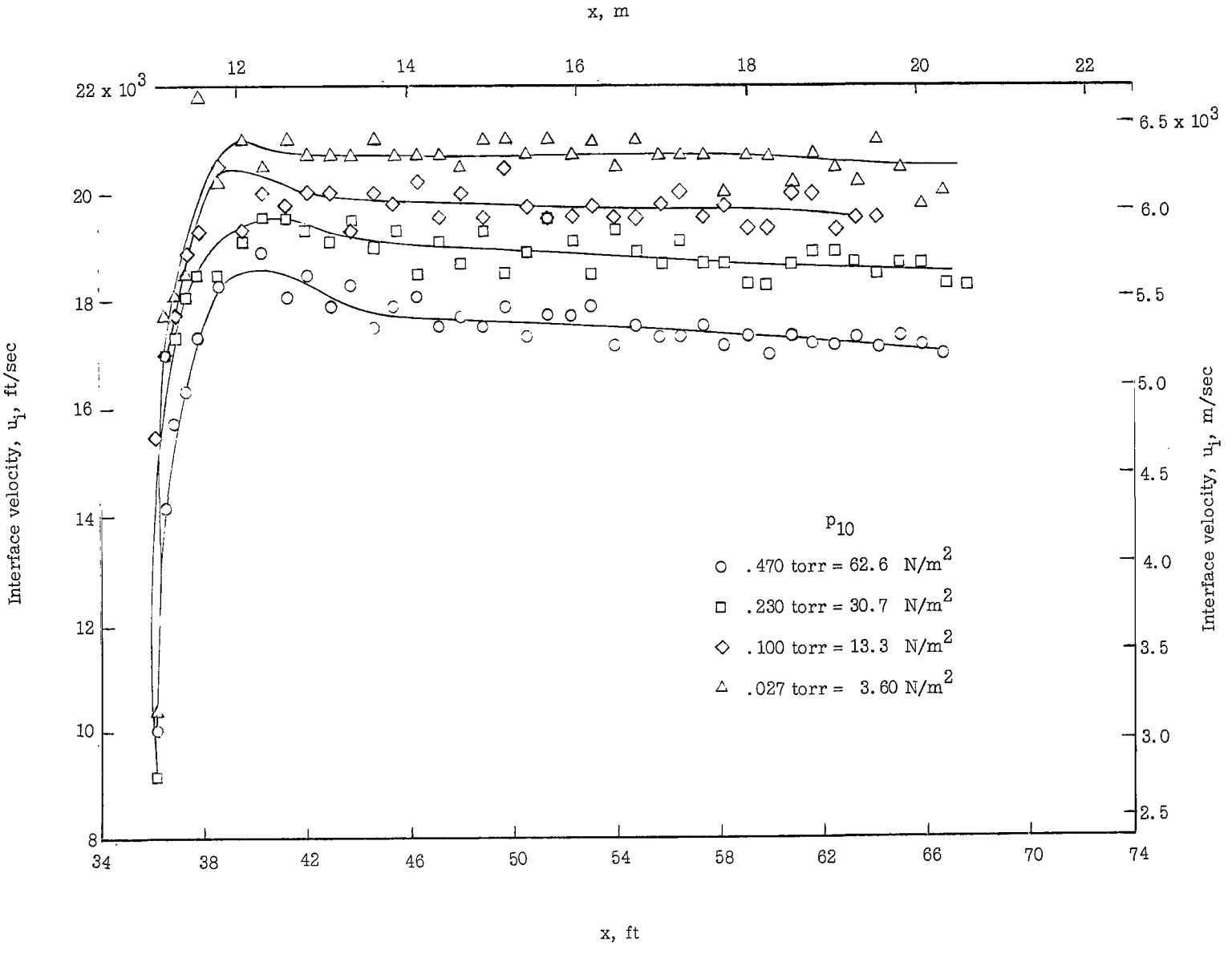

Figure 10.- Interface velocity as determined by microwave signal for several values of p_{10}. p_1 = 22 torr = 2933 N/m^2.

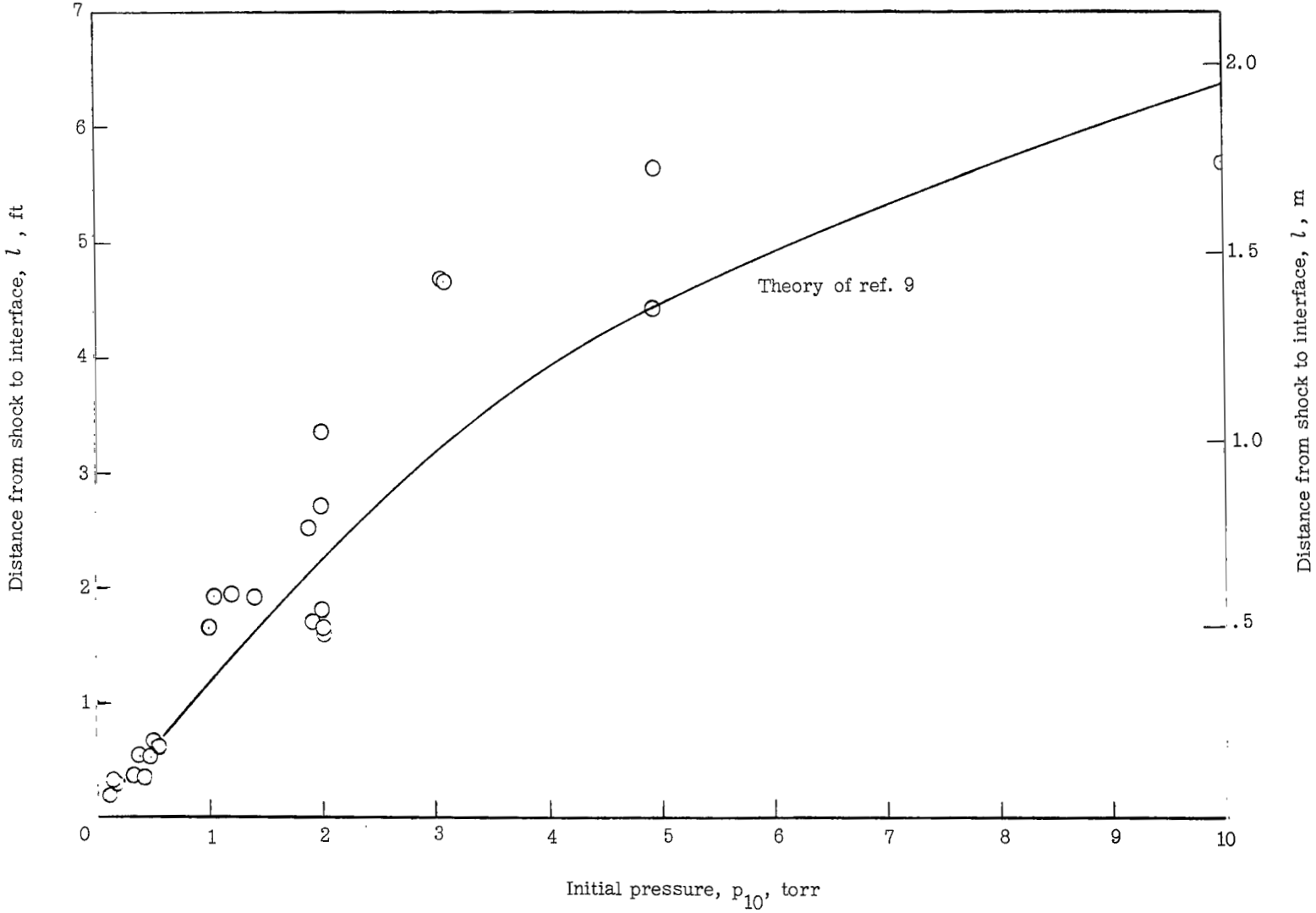

Figure 11.- Comparison of theory and experiment for shock-interface separation at a location 45 feet (13.72 m) from the second diaphragm.

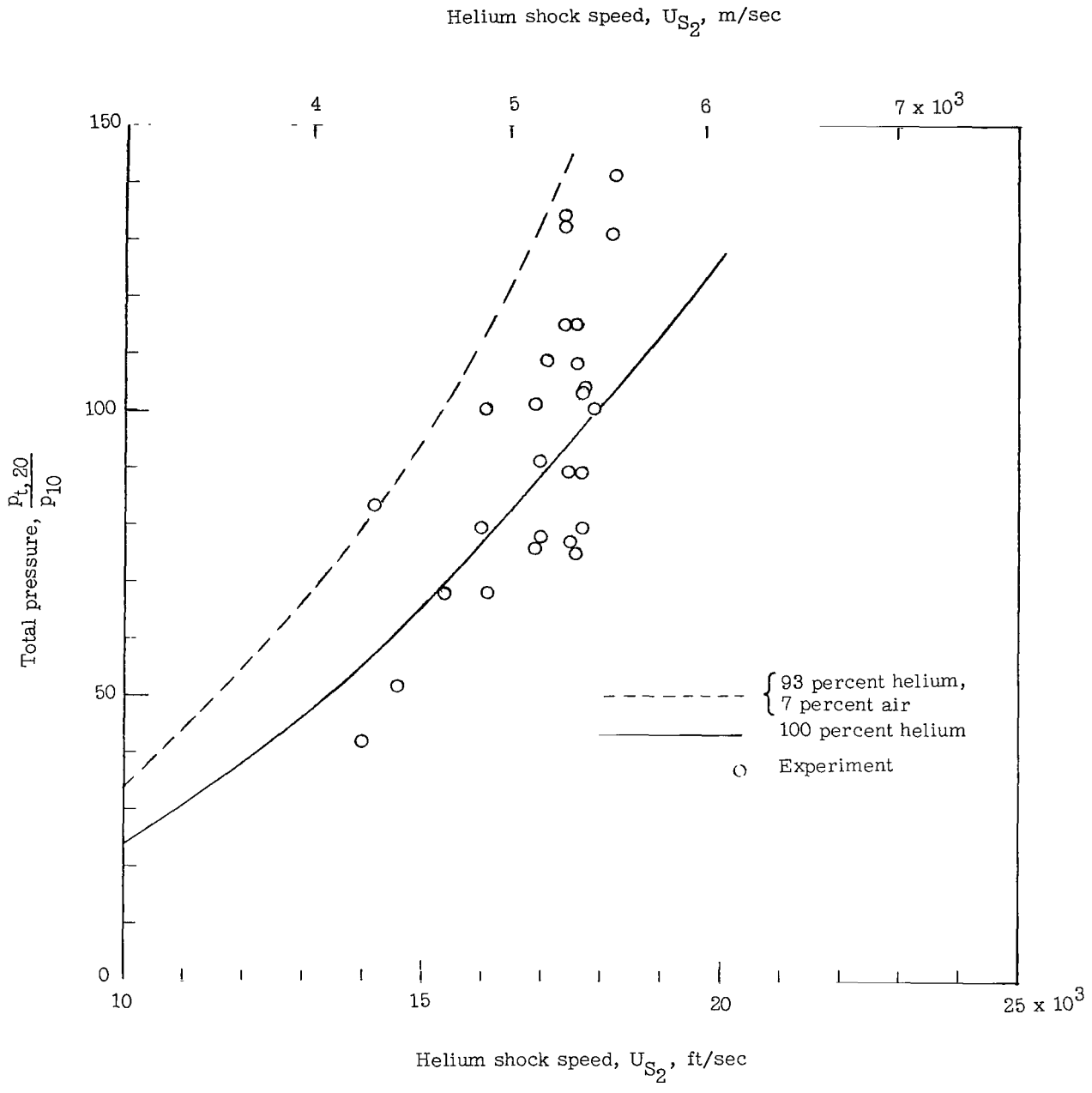

Figure 12.- Pitot pressure in helium flow.

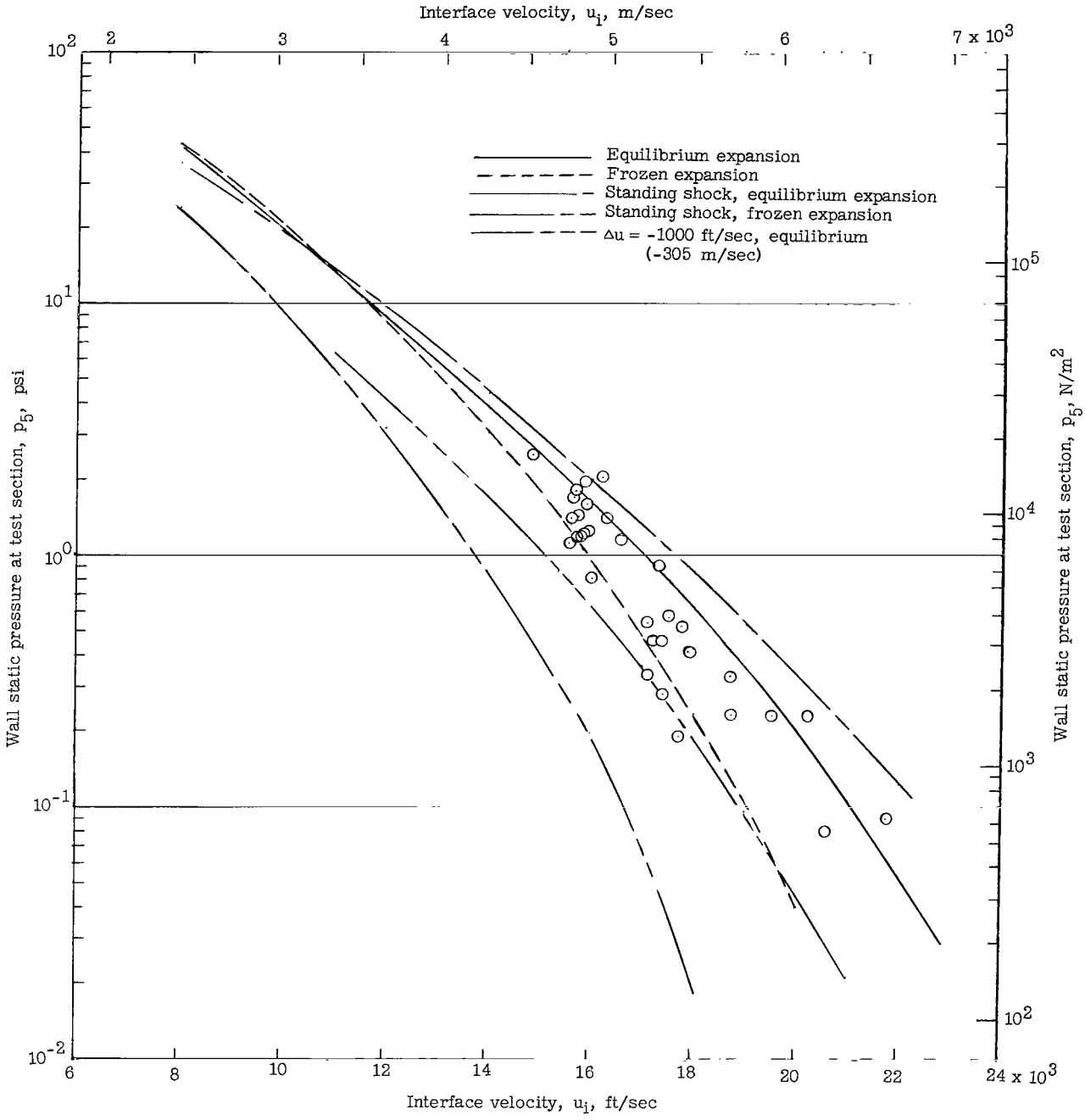

(a) p_1 = 22 torr = 2933 N/m^2.

Figure 13.- Experimental wall static pressure at test section compared with several theoretical assumptions.

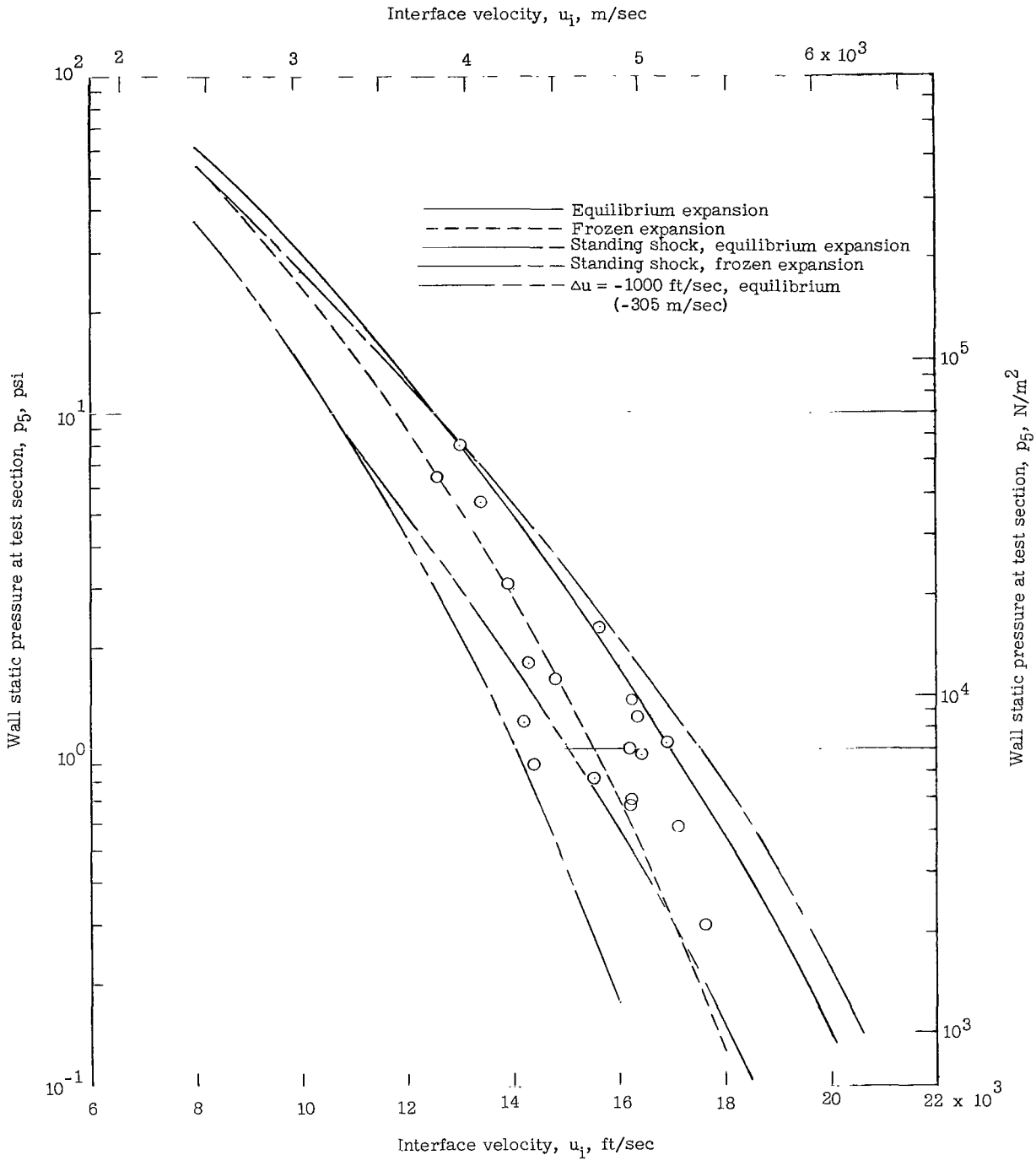

(b) p_1 = 50 torr = 6666 N/m^2.

Figure 13.- Continued.

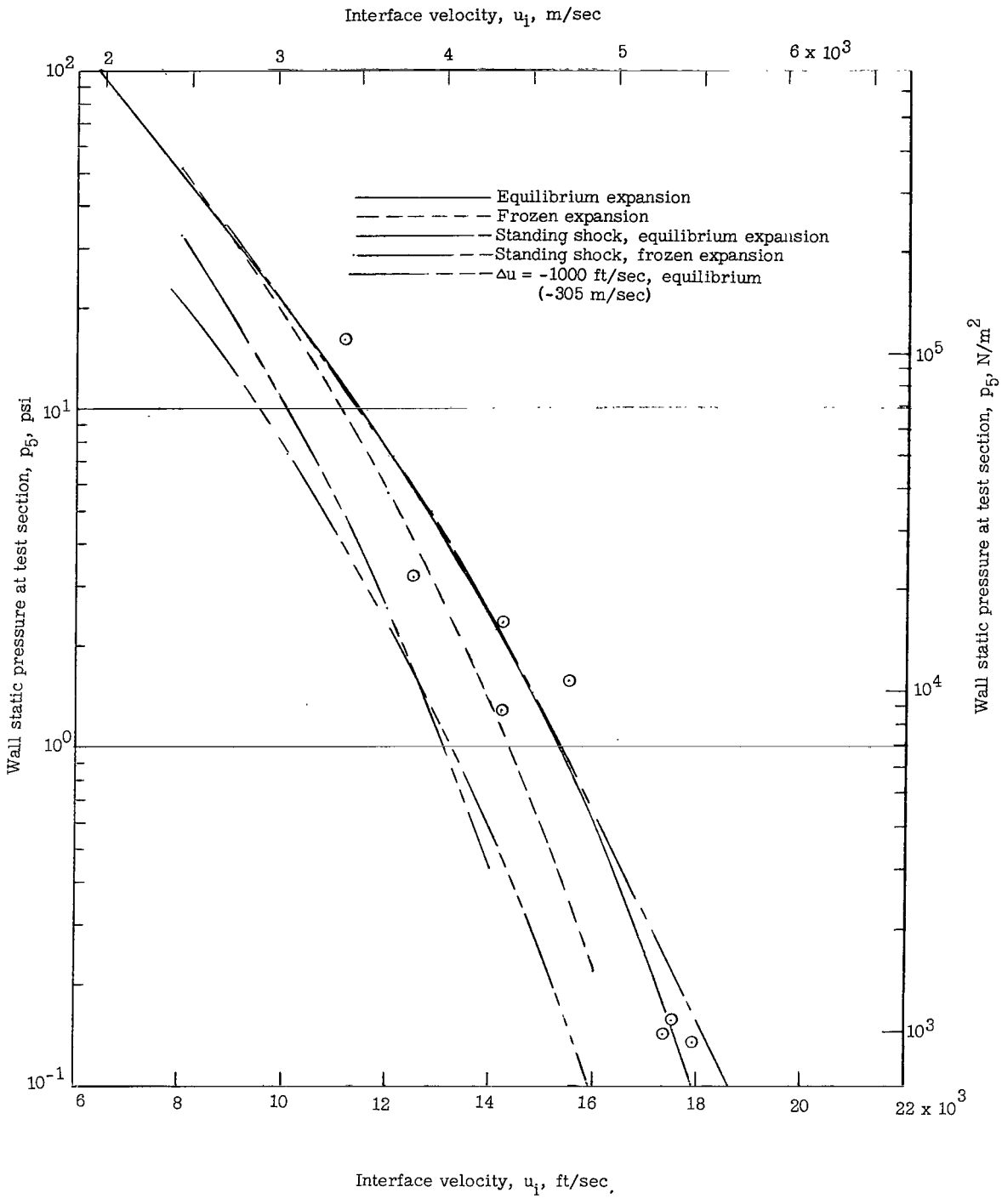

(c) p_1 = 100 torr = 13 332 N/m^2.

Figure 13.- Concluded.

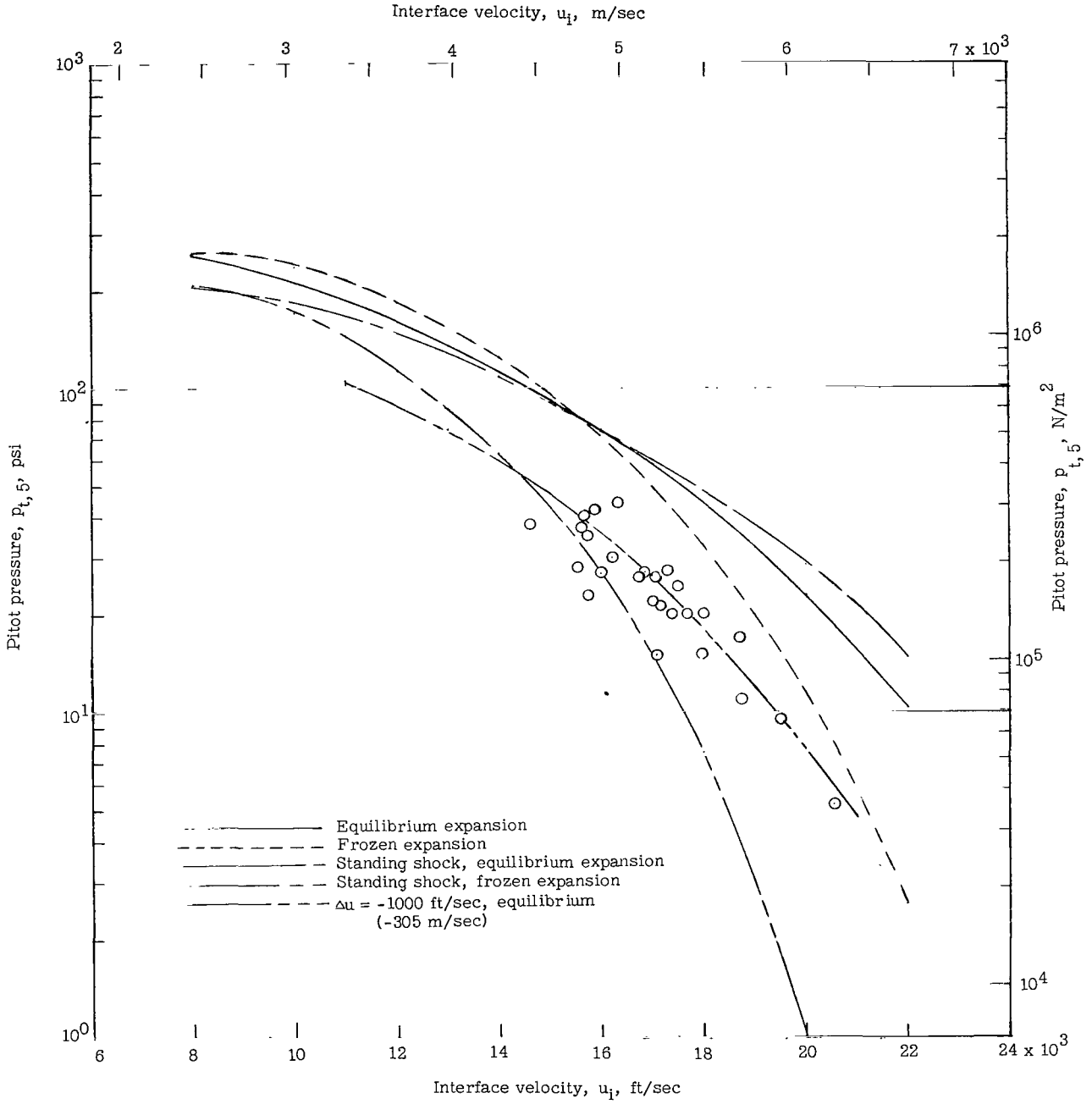

(a) p_1 = 22 torr = 2933 N/m^2.

Figure 14.- Comparison of calculated and measured pitot pressures.

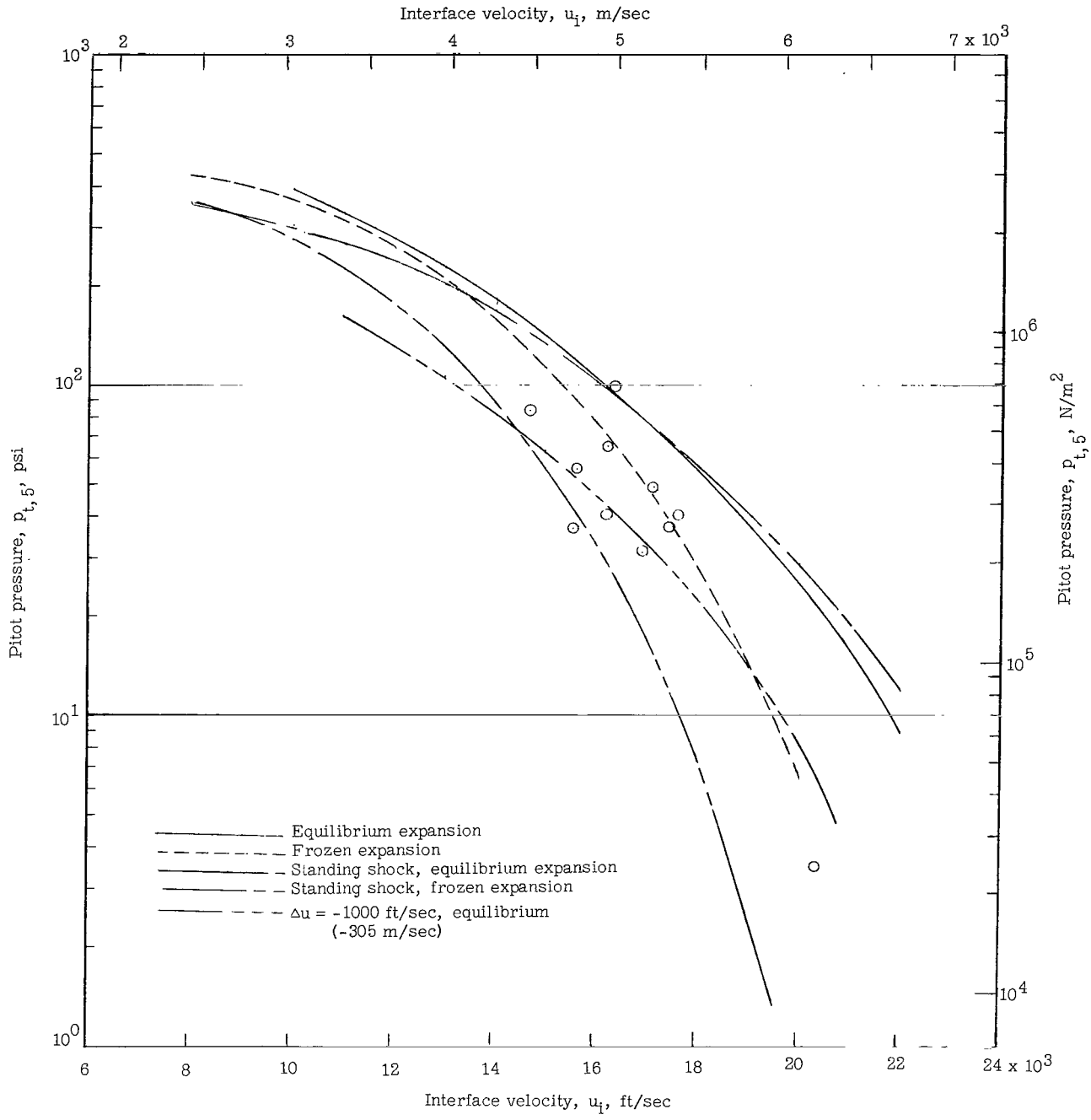

(b) p_1 = 50 torr = 6666 N/m^2.

Figure 14.- Continued.

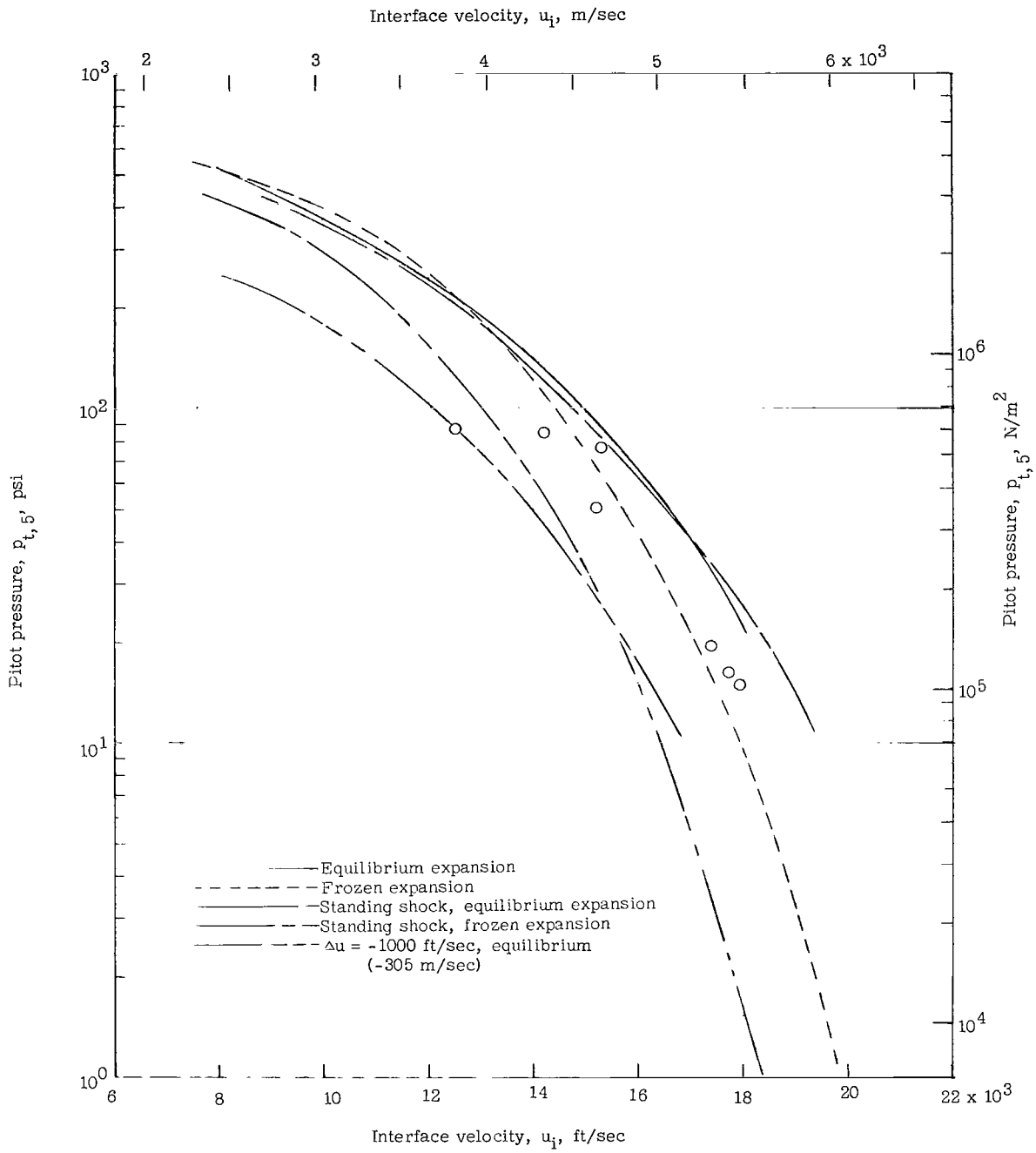

(c) p_1 = 100 torr = 13 332 N/m^2.

Figure 14.- Concluded.

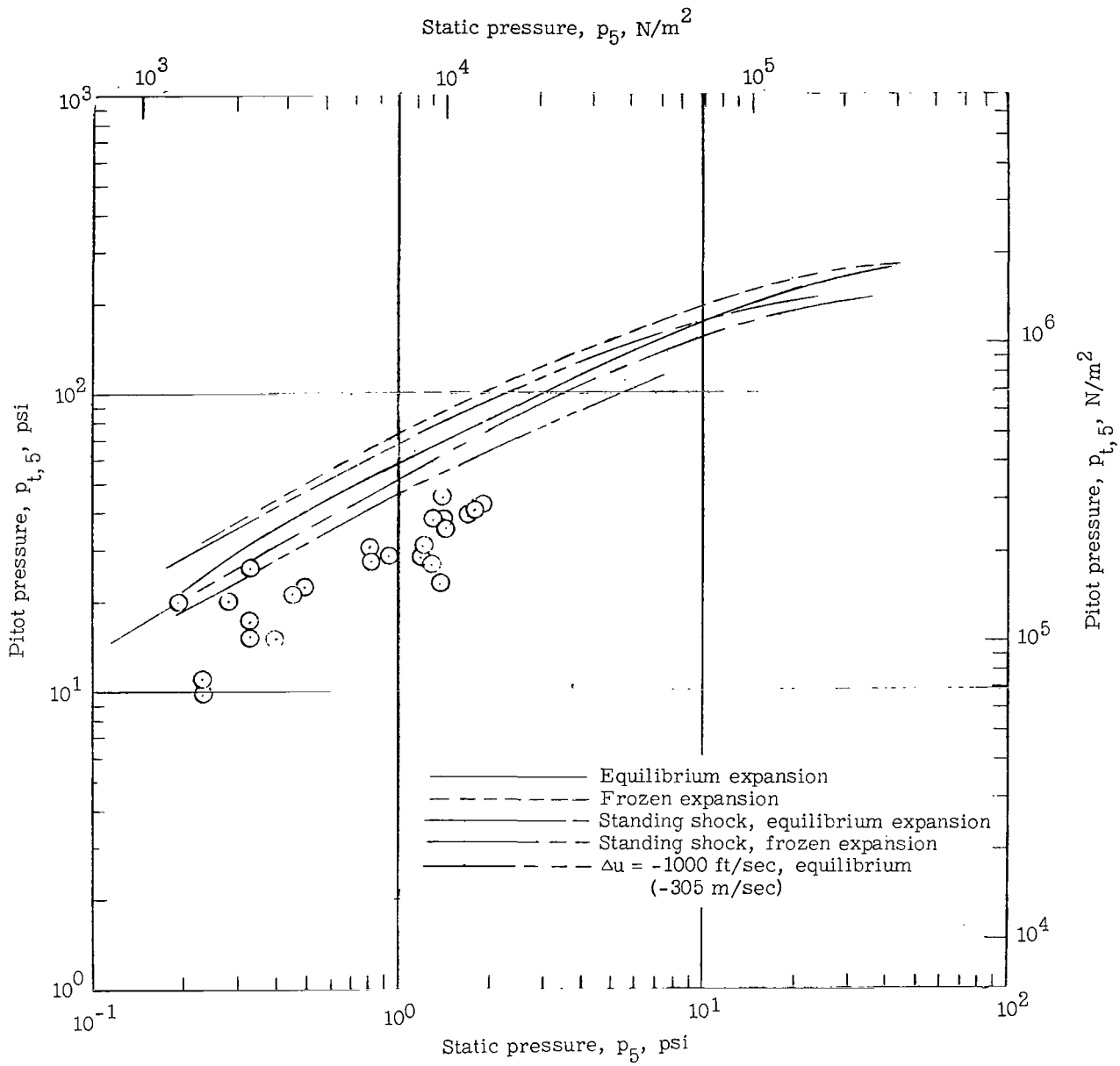

(a) p_1 = 22 torr = 2933 N/m^2.

Figure 15.- Experimental variation of pitot pressure with static pressure and comparison with theory.

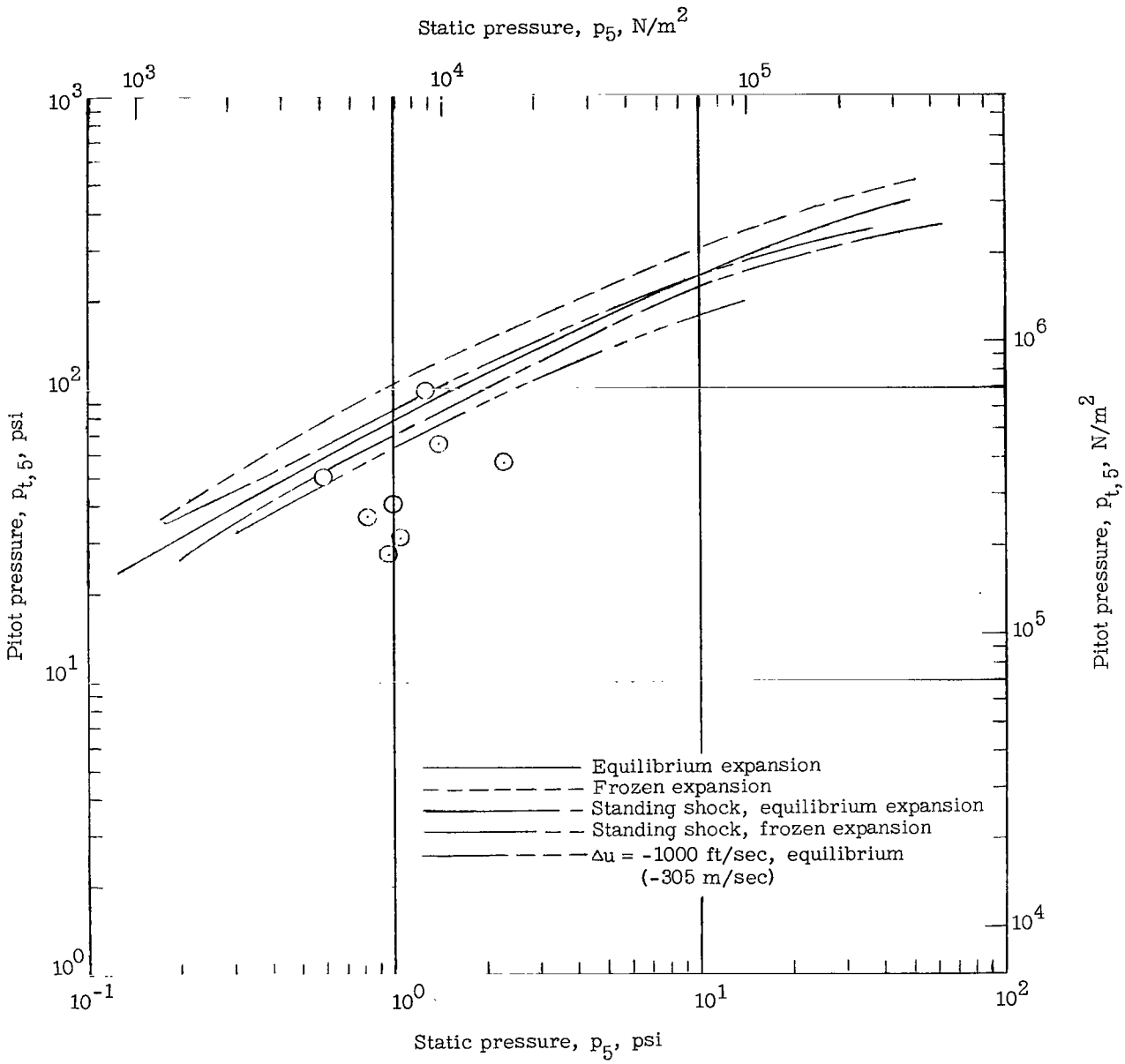

(b) p_1 = 50 torr = 6666 N/m^2.

Figure 15.- Continued.

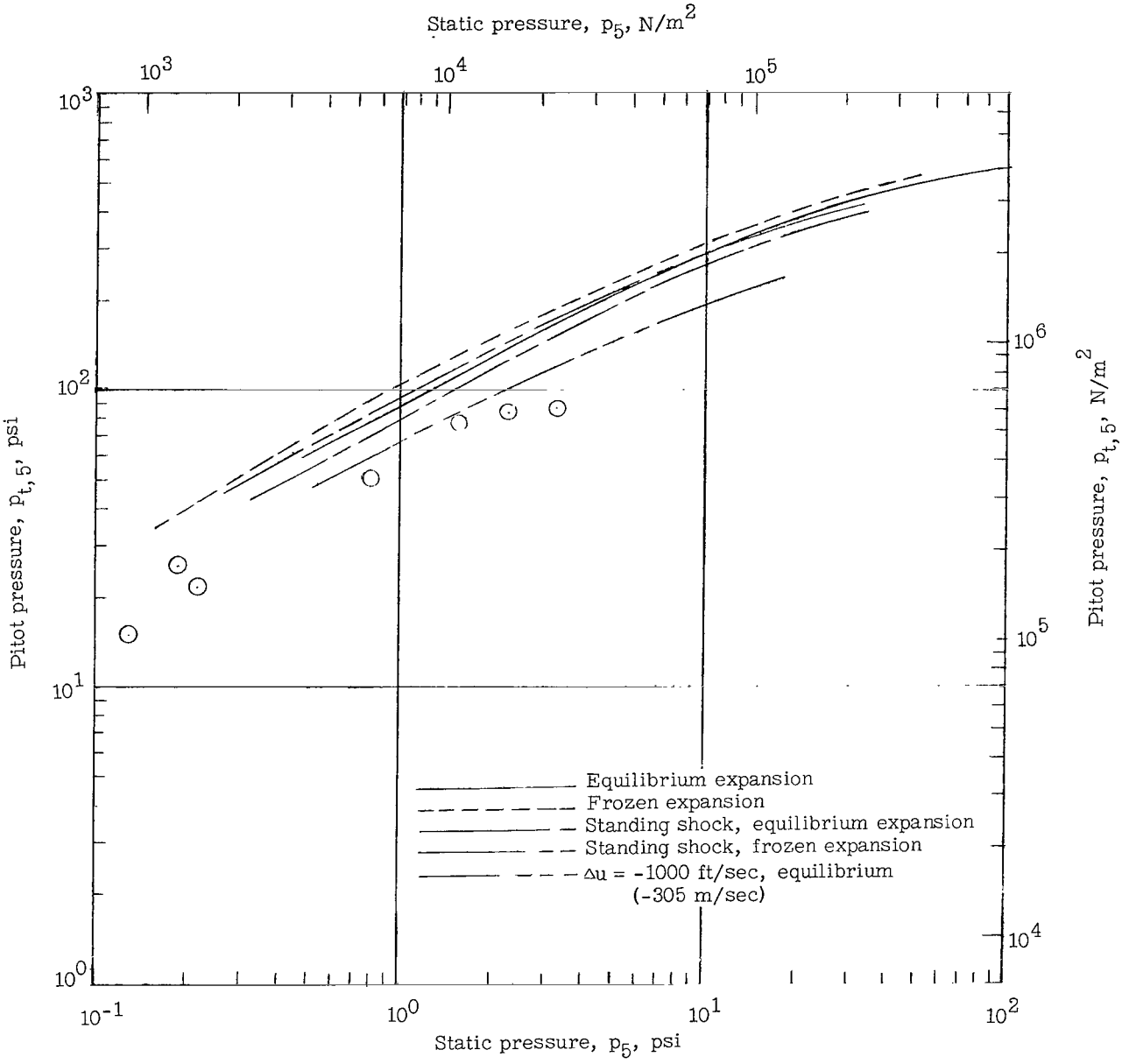

(c) p_1 = 100 torr = 13 332 N/m^2.

Figure 15.- Concluded.

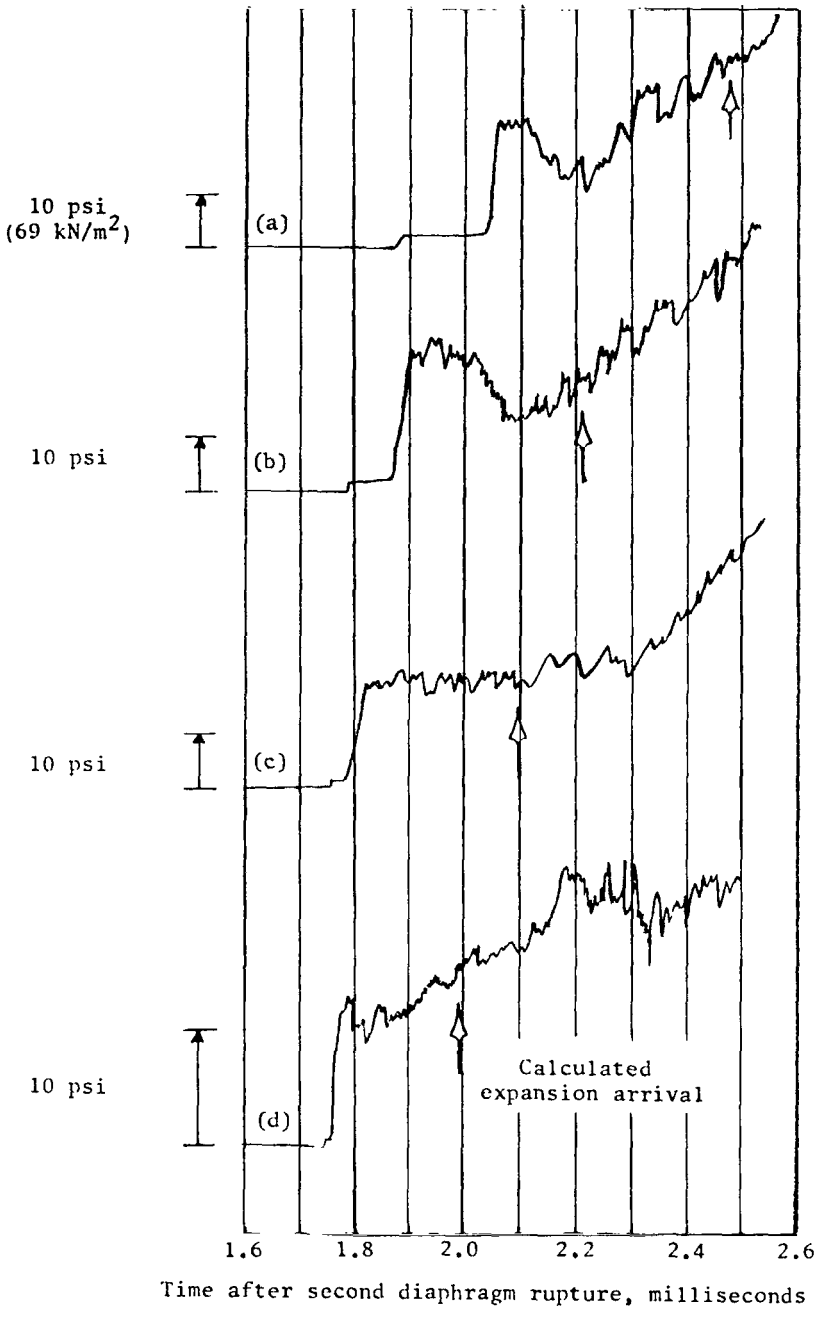

(a) p_{10} = 1.98 torr = 264 N/m^2.

(b) p_{10} = 0.95 torr = 127 N/m^2.

(c) p_{10} = 0.45 torr = 60.0 N/m^2.

(d) p_{10} = 0.095 torr = 12.7 N/m^2.

Figure 16.- Pitot-pressure tracings showing effect of varying acceleration-chamber pressure p_{10}.

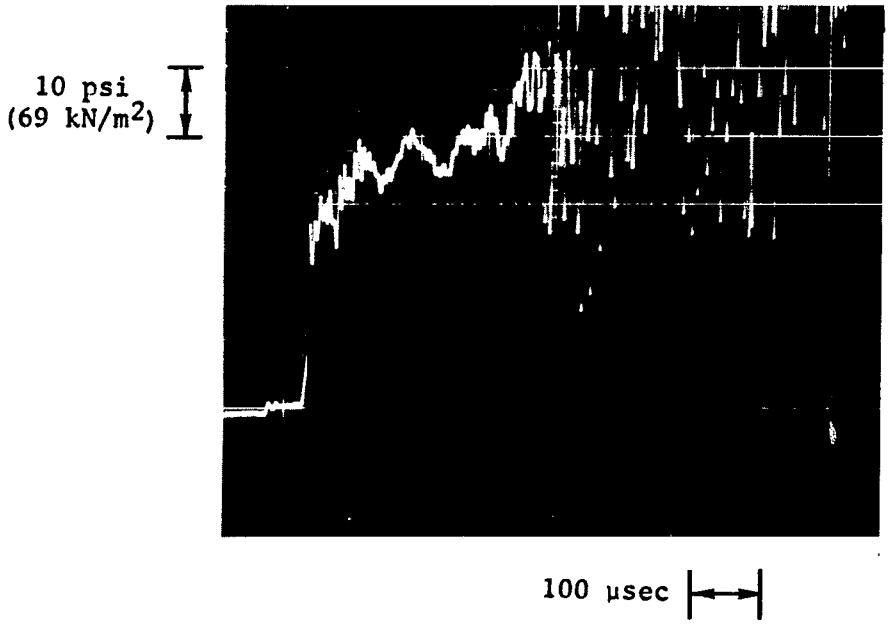

(a) Expansion-tube pitot pressure. p_1 = 50 torr; p_{10} = 0.70 torr.

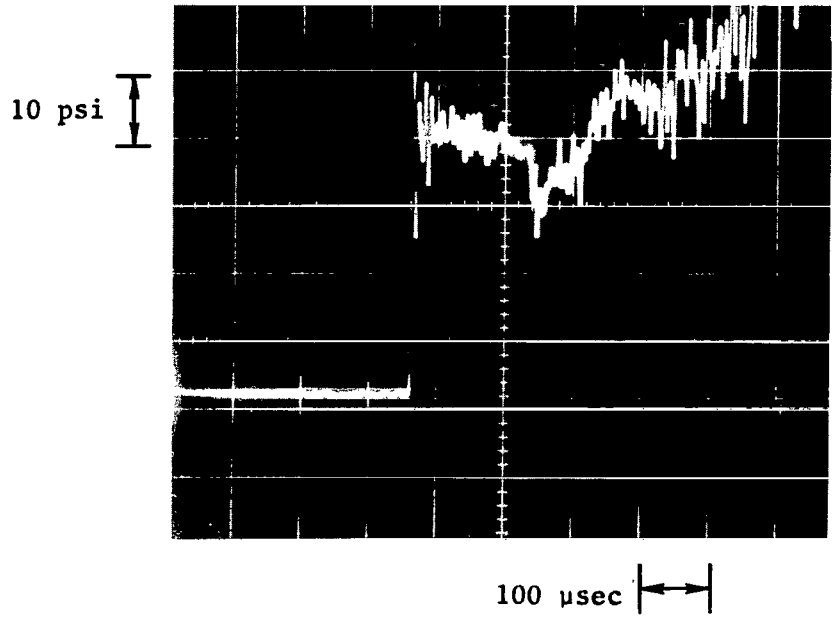

(b) Shock-tube pitot pressure. p_1 = 1.95 torr.

Figure 17.- Comparison of noise induced on pitot-pressure transducer in expansion-tube and shock-tube flows.

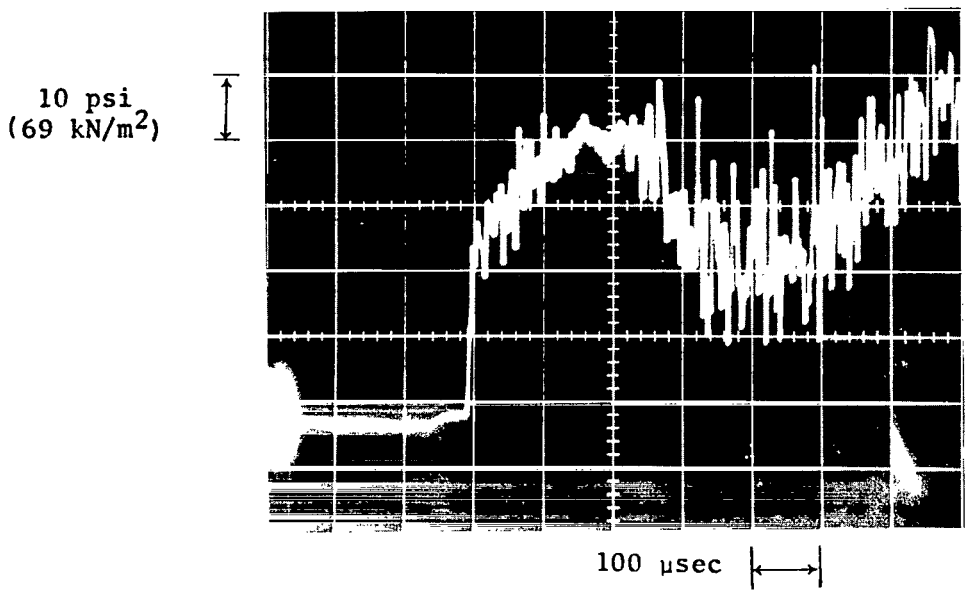

(a) Pitot pressure.

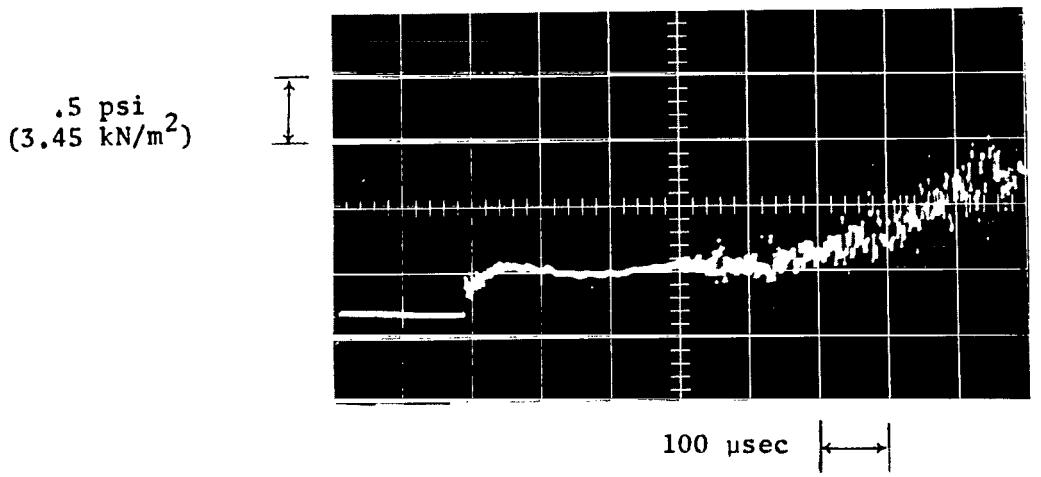

(b) Wall static pressure.

Figure 18.- Comparison of wall static and pitot pressures for expansion-tube flow. p_1 = 50 torr; p_{10} = 0.70 torr.

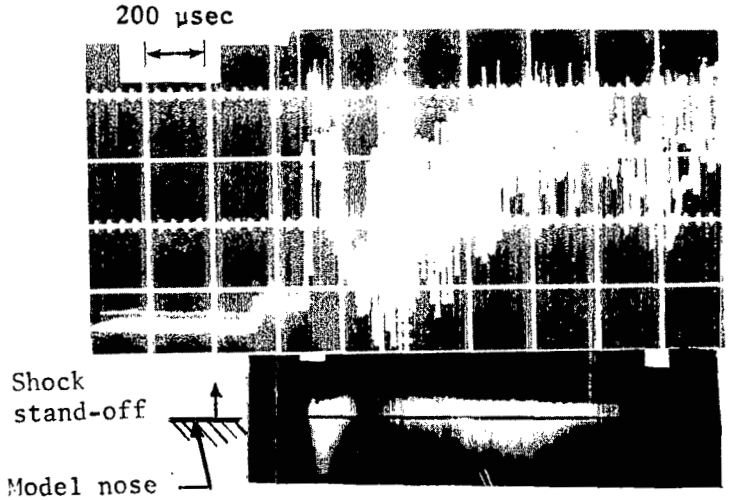

(a) p_{10} = 2.0 torr; PET diaphragm.

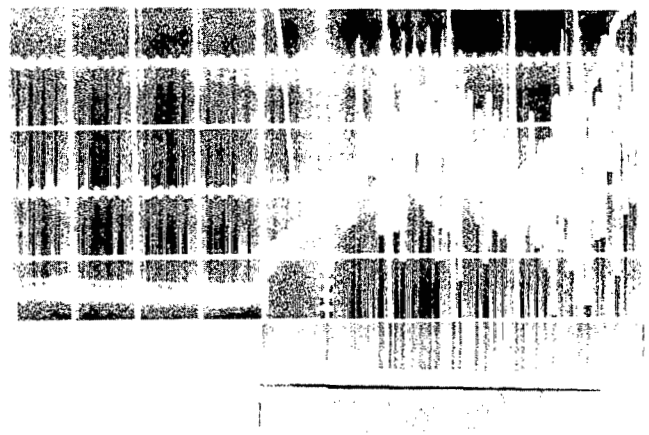

(b) p_{10} = 2.0 torr; wax-paper diaphragm.

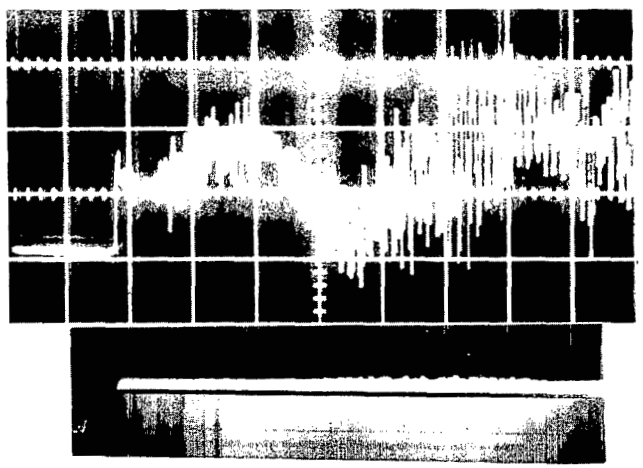

(c) p_{10} = 0.13 torr.

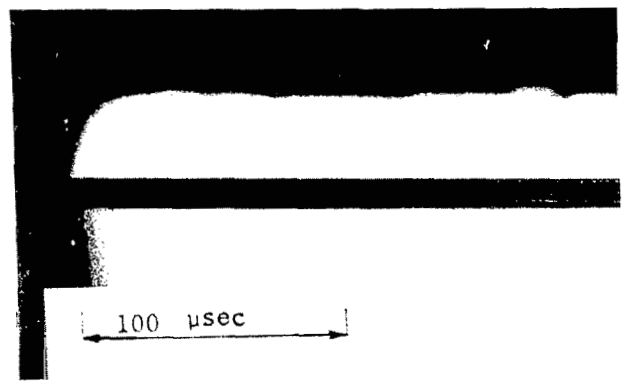

(d) Enlarged view of (c).

Figure 19.- Sample streak-camera records of shock stand-off distance with accompanying pitot-pressure oscillograms reproduced to the same time scale. p_t = 10 psi/cm (68.9 kN/m^2/cm); sweep, 200 μsec/cm.

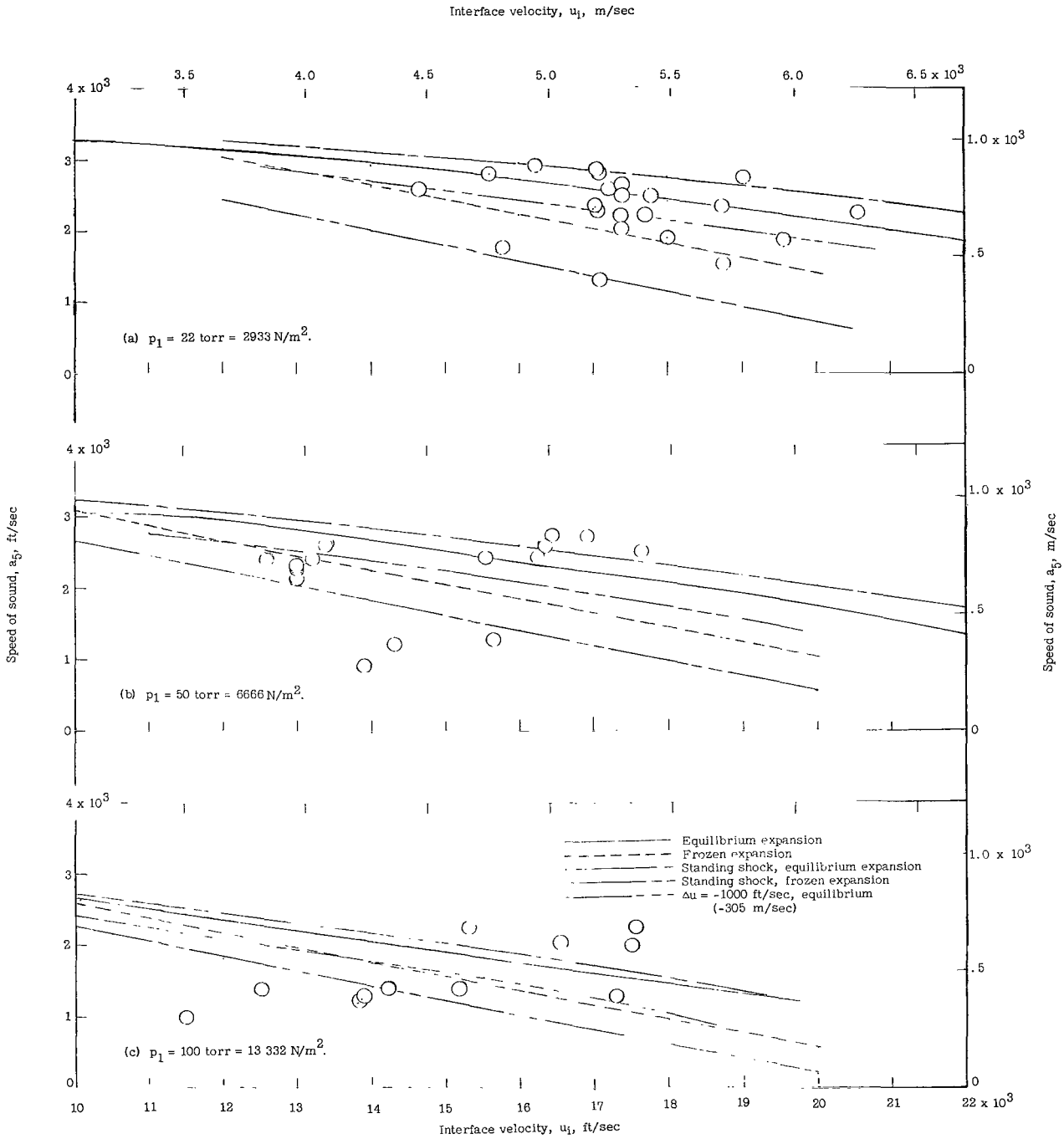

Figure 20.- Sound-speed measurements inferred from expansion-tail velocity as a function of flow velocity.

"The aeronautical and space activities of the United States shall be conducted so as to contribute . . . to the expansion of human knowledge of phenomena in the atmosphere and space. The Administration shall provide for the widest practicable and appropriate dissemination of information concerning its activities and the results thereof."

—NATIONAL AERONAUTICS AND SPACE ACT OF 1958

NASA SCIENTIFIC AND TECHNICAL PUBLICATIONS

TECHNICAL REPORTS: Scientific and technical information considered important, complete, and a lasting contribution to existing knowledge.

TECHNICAL NOTES: Information less broad in scope but nevertheless of importance as a contribution to existing knowledge.

TECHNICAL MEMORANDUMS: Information receiving limited distribution because of preliminary data, security classification, or other reasons.

CONTRACTOR REPORTS: Technical information generated in connection with a NASA contract or grant and released under NASA auspices.

TECHNICAL TRANSLATIONS: Information published in a foreign language considered to merit NASA distribution in English.

TECHNICAL REPRINTS: Information derived from NASA activities and initially published in the form of journal articles.

SPECIAL PUBLICATIONS: Information derived from or of value to NASA activities but not necessarily reporting the results of individual NASA-programmed scientific efforts. Publications include conference proceedings, monographs, data compilations, handbooks, sourcebooks, and special bibliographies.

Details on the availability of these publications may be obtained from:

SCIENTIFIC AND TECHNICAL INFORMATION DIVISION

NATIONAL AERONAUTICS AND SPACE ADMINISTRATION

Washington, D.C. 20546